INSTITUT DE FRANCE
Académie des sciences

Comptes Rendus

Géoscience

Sciences de la Planète

Violaine Sautter and Valerie Payre

Alkali magmatism on Mars: an unexpected diversity

Volume 353, Special Issue S2 (2021), p. 61-90

Published online: 8 September 2021
Issue date: 28 January 2022

https://doi.org/10.5802/crgeos.64

Part of Special Issue: Perspectives on alkaline magmas
Guest editor: Bruno Scaillet (Institut des Sciences de la Terre d'Orléans, CNRS, France)

Les Comptes Rendus. Géoscience — Sciences de la Planète *sont membres du Centre Mersenne pour l'édition scientifique ouverte*
www.centre-mersenne.org
e-ISSN : 1778-7025

Comptes Rendus
Géoscience — Sciences de la Planète
2021, 353, nº S2, p. 61-90
https://doi.org/10.5802/crgeos.64

Perspectives on alkaline magmas / *Perspectives sur les magmas alcalins*

Alkali magmatism on Mars: an unexpected diversity

Violaine Sautter *, [a] **and Valerie Payre** [b, c]

[a] IMPMC-UMR, CNRS7590-Sorbonnne Université, 61 rue Buffon, 75231 Paris, France

[b] Rice University, Houston, TX77005-1892, USA

[c] Department of Physics and Astronomy, Northern Arizona University, Flagstaff, AZ 86011, USA

E-mails: violaine.sautter@mnhn.fr (V. Sautter), valerie.payre@nau.edu (V. Payre)

Abstract. Despite an apparent north/south topographic dichotomy that formed >4.0 Ga, the young Martian meteorites (<2.4 Ga) and first-order remote sensing observations revealed a surface of Mars that is uniformly basaltic. This simplistic vision has been challenged by the discovery of a brecciated meteorite and additional spacecraft data that all point to the presence of alkaline igneous rocks, thereby demonstrating an unexpected igneous diversity on Mars. In the present paper, we review a variety of effusive alkaline rocks (basalts to trachytes) recognized so far in the southern hemisphere of Mars as observed from a unique 4.47 Ga Martian meteorite, as well as ground, and orbital data. The complementary of effusive alkaline rocks and plutonic orthopyroxene-rich rocks in early Mars is discussed. We propose that mantle-derived magmas at high extent of melting at rather low pressure either erupted forming orthopyroxene-rich lavas, or crystallized at shallow crustal depths, fractionating orthopyroxene which sank to the bottom of the chamber and residual alkaline magmas which erupted at the surface of Mars. Widespread low pressure fractionation processes could also be related to heavy bombardment on the early Martian crust generating melt sheets that ultimately differentiated. The Noachian crust is more diverse than being merely basaltic.

Keywords. Mars, Martian meteorite, Orbital spacecraft, In situ rover, Noachian crust, Alkaline igneous trend.

Available online 8th September 2021

1. Introduction

The chemistry and mineralogy of the Martian surface have increasingly been better constrained these past 40 years thanks to Martian meteorites and remote analyses obtained by rovers, landers, and orbiting spacecraft. All the data sets available from Mars until 2012 were in agreement with a homogeneous basaltic Martian crust with a Fe-rich tholeiitic composition [McSween et al., 2003, 2009, McSween, 2015, Udry et al., 2020], consistent with liquids produced by partial melting of the mantle and transport of those magmatic liquids toward the surface [Baratoux et al., 2011, 2013]. The simple view of Mars being a basalt-covered world had been challenged these past ten years by recent observations of differentiated rocks that combine new Martian meteorite finds [Agee et al., 2013, Humayun et al., 2013, Santos et al., 2015, Hewins et al., 2017], remote analyses from the Mars Science Laboratory (MSL) *Curiosity* rover [Cousin et al., 2017, Payré et al., 2020, Sautter et al., 2016, 2015, 2014, Stolper et al., 2013], and spectroscopic

* Corresponding author.

signatures observed from orbit by visible and very near infrared [Carter and Poulet, 2013, Wray et al., 2013]. Most orbital and ground observations of evolved felsic igneous rocks are located in the southern hemisphere that concentrates the most ancient terrains (3.5–4.5 Ga). The geoid to topographic ratios calculated from orbital data also question the basaltic nature of the crust, suggesting buried felsic crustal components beneath the mafic surface in the southern hemisphere, [Baratoux et al., 2014, Sautter et al., 2016, Wieczorek and Zuber, 2004]. As a whole, the large variations in silica and alkali contents within igneous rocks throughout the ancient southern hemisphere expand the diversity of the magmatic history on Mars and highlight its complexity, especially in ancient times.

In this chapter, we will review the occurrence of alkali-rich igneous rocks recognized so far on Mars. We will then discuss potential scenarios including the nature of crystallization processes producing alkaline rocks on Mars. Finally, such differentiated magmatism in a terrestrial planet such as Mars without plate tectonics (i.e. in a stagnant lid system) will be discussed.

2. Martian geology at planetary scale as seen from orbit

Martian geology has been studied in the last decades through an increasing number of orbital spacecraft. Orbital observations of the Martian crust have been performed at a number of different spatial scales using a variety of remote sensing techniques, each of which provides different but complementary information such as the topography, mineralogy, and chemistry of surface materials.

The Mars Orbiter Laser Altimeter (MOLA) onboard the Mars Global Surveyor spacecraft revealed one of the first evident features when looking at a global map of Mars, which is the topographic dichotomy between the northern hemispheric lowlands and the southern hemispheric highlands (Figure 1a). Examining the map closer, highly craterized highlands stand out from smooth lowlands (Figure 1a). Counting craters and inferring the density of craters following lunar crater density regressions enable geologists to date the surface of Mars (Figure 1b [Carr and Head, 2010, Hartmann and Neukum, 2001]. Martian time is divided into four main periods, pre-Noachian >4.1 Ga, Noachian 4.1–3.7 Ga, Hesperian 3.7–3.2 Ga, and Amazonian 3.2 Ga—today (Figure 1b). The topographic dichotomy is associated with an age dichotomy, with the highly craterized highlands in the southern hemisphere concentrating ancient terrains >3.5 Ga, older than most terrestrial surfaces where Archean terrains are less than 6%, and the smooth lowlands in the northern hemisphere presenting younger surfaces <3.7 Ga [Wyatt et al., 2004]. Overall, the vast majority of the southern highlands are dominated by brecciated terrains that are mid-Noachian in age (3.95–3.8 Ga) and a few scattered patchy areas of early Noachian age (4.1–3.95 Ga) such as the Cimmeria–Sirenum massif.

The Gamma-Ray Spectrometer (GRS) onboard the Mars Odyssey spacecraft measures the surface geochemistry. GRS measurements and global distribution maps have been published for potassium, thorium, iron, silicon, chlorine, and hydrogen [Boynton et al., 2007], and more recently aluminum [Karunatillake et al., 2009] and sulfur [Karunatillake et al., 2014; Table 1]. The GRS instrument typically samples the first tens of centimeter below the surface avoiding the analyses of dust and surface coating, which is convenient for a dusty world such as Mars. GRS elemental maps are convenient when evaluating the nature of Mars surface, but the spatial resolution is low, being approximately equal to the spacecraft altitude (~300 km/pixel; Table 1). With such a resolution, where large 150–200 km diameter craters are represented by one-half pixel only, the crustal composition of both hemispheres appears to be homogeneous, by definitely missing compositional anomalies that are less than tens of kilometers in scale. Measurements indicate that the first tens of centimeters below the surface of Mars has a SiO_2 composition ranging from 39 to 50 wt%, suggesting that mafic rocks are volumetrically dominant. All volcanic provinces identified by GRS are at first order uniformly basaltic [Taylor et al., 2010, Baratoux et al., 2011]. Although basaltic in composition, some terrains are more concentrated in Si, K and Th (Si > 19.9 wt%, K > 0.38 wt%, Th > 0.57 ppm) and more depleted in Fe (Fe < 15.4 wt%) than elsewhere. Combining the Si, Fe, K, and Th abundance maps [Figure 2; Boynton et al., 2007] with a geological age map [Tanaka et al., 2014] highlights six distinct regions enriched in incompatible elements (Th and K "hotspots") located in the

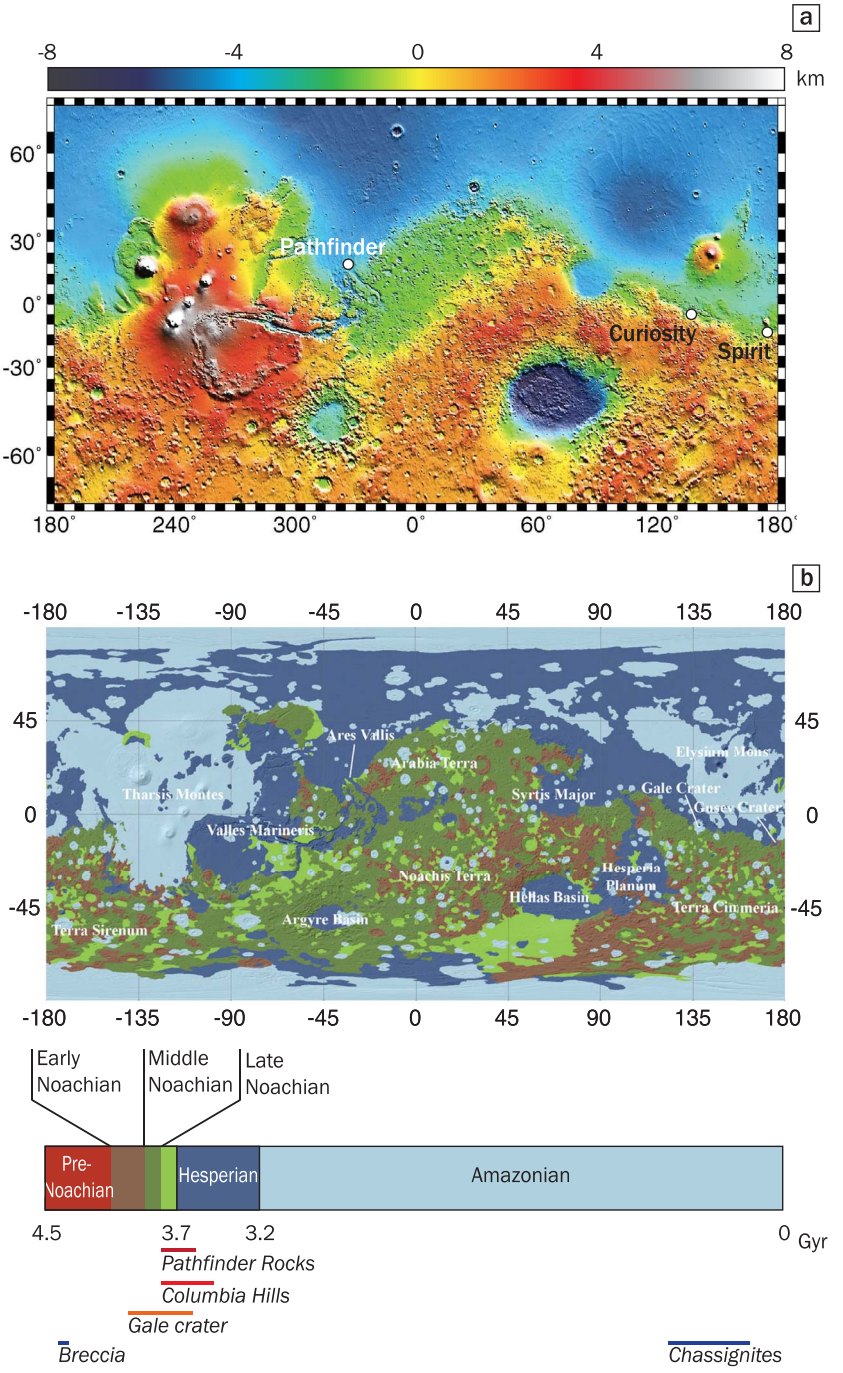

Figure 1. (a) MOLA (Mars Orbital Laser Altimeter) relief topographic global map of Mars. (b) Simplified chronostratigraphic map from Tanaka et al. [2014], with the age of crystallization of alkaline materials observed at the surface of Mars and in the Martian meteorites. Note that the early Noachian units are sparse and that the middle Noachian unit is the most common unit of Noachian terrains.

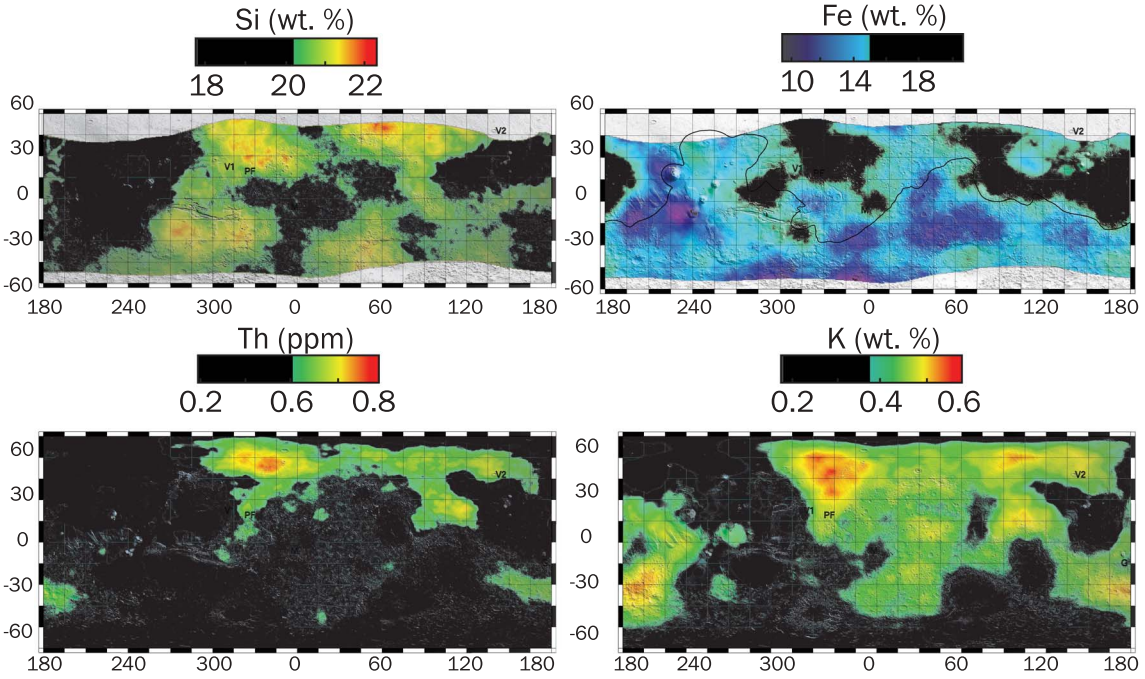

Figure 2. Mars Odyssey Gamma-Ray Spectrometer (GRS) data for the abundance of Si, Fe, Th and K displayed over a shaded relief of Mars. Colored areas underline terrains containing SiO_2 > 42.6 wt%, K_2O > 0.45 wt%, Th > 0.57 ppm, and FeO < 19.8 wt%—i.e., upper and lower half of the measured compositions, making them relatively Si–K–Th rich and Fe poor in comparison with surrounding terrains. Landing sites are indicated in white: V1—Viking 1; V2—Viking 2; PF—Pathfinder; M—Opportunity in Meridiani Planum; G—Spirit in Gusev Crater; C—Curiosity in Gale.

Table 1. Summary of orbital instruments for measuring the composition and mineralogy of the surface of Mars

	Spatial resolution	Penetration depth	Observation data
GRS	300 km/pixel	Tens of cm	Si, Al, Fe, K, Th, S, Cl, and H
OMEGA	300 m/pixel	0.4–5 μm[a]	Mineralogy
CRISM	18 m/pixel	0.4–4 μm[a]	Mineralogy
TES	3 km/pixel	6–50 μm[a]	Mineralogy and thermal inertia
THEMIS	100 m/pixel	7–15 μm[a]	Thermal inertia and qualitative composition/mineralogy

[a]From Ehlmann and Edwards [2014].

southern hemisphere and dated at early–mid-Noachian (yellow areas in Figure 3): (1) **Terra Tyrrhena** on the north of Hellas Planita at 60–70° W/15° S ; (2) **Xanthe Terra** 1 located more in the north at 50°–45° W/−5°–5° S; (3) **Xanthe Terra 2** slightly on the north of Valles Marineris 50° W/10° S; (4) **Noachis Terra** located between Argyre Planitia and Hellas Planitia impact basins 15° E/50° S; (5) **Terra Sirenum** 170°–165° W/30°–50° S near the landing site of the Soviet Mars 3 mission; (6) **Terra Cimmeria** located on the south of the renowned volcanic region Elysium Planitia between 135° E/15° S and 165° E/40° S. The low spatial resolution raise questions about whether such "hot spots" are related to regional exposures of igneous bedrock, to spatial averaging of sedimentary rocks, or both.

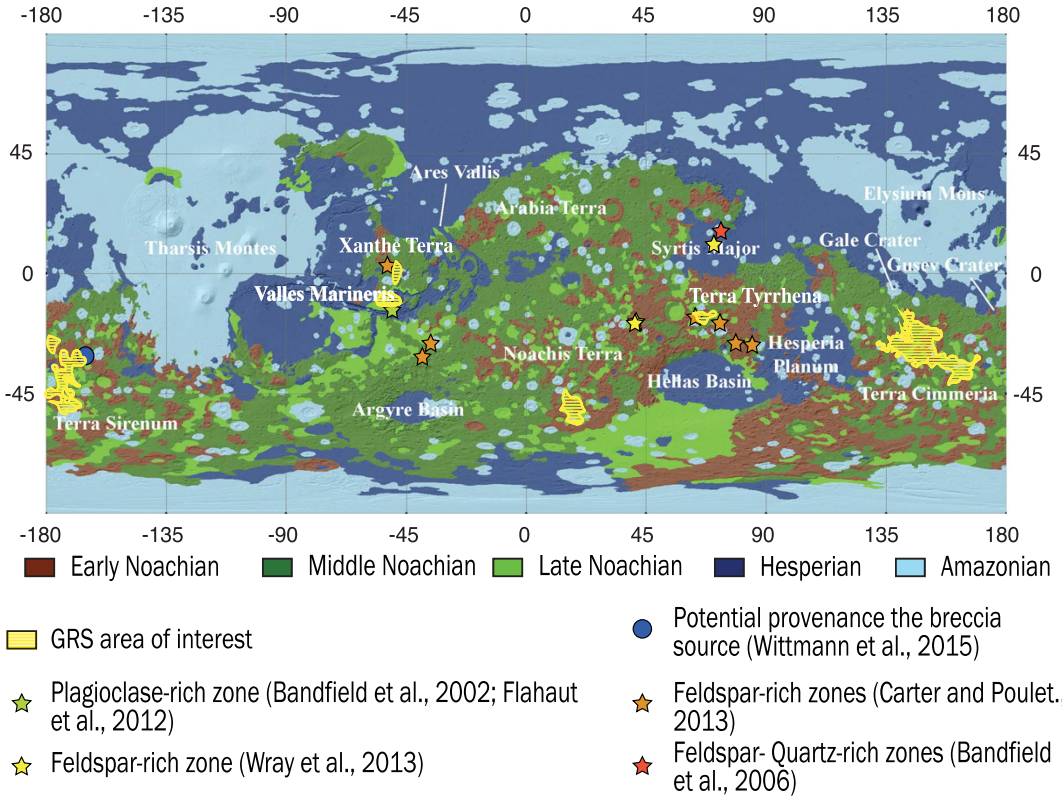

Figure 3. Simplified geological map from Tanaka et al. [2014] where yellow-hatched areas correspond to early Noachian terrains relatively Si–K–Th rich as presented in Figure 5. Colored stars indicate Noachain terrains where feldspar-rich rocks have been detected with orbital instruments (CRISM and TES).

The diagnosis of basaltic dominance at the subsurface is supported as well by mineral mapping provided by optical and infrared spectroscopy (visible and near infrared (VNIR): OMEGA and CRISM [Bibring, 2005, Murchie et al., 2007]; thermal infrared (TIR): TES and THEMIS [Christensen et al., 2001, 2004; Table 1]. They provide measurements of Martian surface at high spatial resolution compared to GRS (Table 1): TES 3 km/pixel; OMEGA 300 m/pixel; THEMIS 100 m/pixel; and CRISM 18 m/pixel. At first glance, the mineralogy of the southern hemisphere is dominated by mafic mineral associations including olivine [Koeppen and Hamilton, 2008], low-Ca pyroxene (LCP corresponding to orthopyroxene and pigeonite) and high-Ca pyroxene (HCP corresponding to augite, diospide, and hedenbergite) making Mars appear to be covered by basaltic lava flows [Christensen et al., 2005, Hamilton et al., 2005, Poulet et al., 2009, Ody et al., 2013, Riu et al., 2019]. Note that the distinction between the different kinds of pyroxene referred to as LCP and HCP using near infrared and thermal infrared spectroscopy is difficult to assess. Observations of pyroxene repartition throughout the planet indicate the pronounced contribution of LCP in ancient terrains at a similar or higher level than that of HCP. This contrasts with younger locations where LCP is virtually absent [Mustard et al., 2005, Poulet et al., 2009]. Such mineral mapping provides a biased petrographic perception of the crust. First of all, the principal pitfall of infrared spectroscopic techniques is a small penetration depth (typically a few microns for VNIR and several μm for TIR; Table 1). The dust cover and/or secondary coatings thus obscure the signature of primary rocks when present. Then, the main felsic igneous minerals like feldspar and quartz are spectrally neutral (transparent) in the visible and VNIR and cannot be detected using this technique

unless the rock contains a limited amount of Fe-rich minerals like olivine and pyroxene [5–40 vol.%; Carter and Poulet, 2013, Rogers and Nekvasil, 2015]. The detection of feldspar is slightly better with thermal infrared spectroscopy as plagioclase shows absorption features in the available spectral range [Hanna et al., 2012], but the spatial resolution of the thermal infrared TES instrument is poor compared to the visible and VNIR CRISM instrument. Orbital spectrometers most likely missed most of the felsic terrains potentially outcropping throughout the southern hemisphere. The detection of feldspar-rich terrains at the surface is therefore overlooked.

Somewhat surprisingly, highly feldspar-rich whitish rocks were identified by visible-VNIR spectroscopy in various scattered Noachian locations in the southern highlands. Some of them are located within the K–Th–Si "hot spots" mentioned above (Figure 3). In **Terra Tyrrhena**, dated from early to mid-Noachian, the CRISM instrument and orbital imaging revealed the occurrence of bright rocks containing 60–95 vol.% of feldspar in a crater rim associated with Al-rich clay, which likely formed from alteration of a felsic outcrop. These have been interpreted as anorthosites [Carter and Poulet, 2013]. Similarly, in a crater rim in **Xanthe Terra** and **Noachis Terra 1**, CRISM data revealed the same kind of formation but these were interpreted as granitoids [Rogers and Nazarian, 2013, Wray et al., 2013].

Close to **Xanthe Terra 2** where CRISM data also revealed light-toned feldspar-rich materials [Wray et al., 2011], the Valles Marineris canyon provides a unique vertical section through time, dated between the early Hesperian at the top and the early Noachian at the bottom. Orbital images revealed light-toned massive bedrock at the bottom of the canyon [Flahaut et al., 2012], which is dominated by LCP according to CRISM data, and large amounts of plagioclases according to TES measurements [~26%; Bandfield, 2002]. [Flahaut et al., 2012] suggest that the LCP-rich light-toned massive rocks are an exposure of a Noachian pristine crust. Large amounts of plagioclases have been revealed by TES analyses, but the spatial resolution of the TES instrument does not allow the precise identification of the nature of the plagioclase-bearing unit [Bandfield, 2002]. Finally, two large areas in **Terra Sirenum** and **Terra Cimmeria**, from early to late Noachian (Figure 3), have been interpreted as a thick 4.2 Ga crustal component that presents the strongest remnant crustal magnetism [Bouley et al., 2020, Connerney et al., 2005]. A geomorphological study revealed early Noachian volcanic edifices likely being shield-like volcanoes with 50–100 km diameter and 2–3 km height [Xiao et al., 2012]. According to these authors, the ancient volcanoes could be the remnants of a larger population that occurred in early Noachian.

Orbital data revealed several Noachian areas scattered throughout the southern hemisphere with both lithophile-rich concentrations and feldspar-rich signatures associated sometimes with kaolin and/or LCP, demonstrating potential early evolved magmatic processes. Although orbital observations are essential to map out some representative minerals at the surface of the planet, imaging and instrumental resolution are insufficient to identify unambiguously the petrography of any Martian outcrop. If LCP are abundant in Noachian terrains, the nature of the host rocks is not established, potentially being basalts, norites, gabbros, or orthopyroxene cumulates. Similarly, it is impossible to distinguish anorthosite rocks from granites or alkaline lava flows, from orbit.

To summarize, all orbital data combined indicate at first order that the magmatic surface of Mars is overall basaltic with LCP/HCP ratio increasing in terrains older than 3.7 Ga. Scattered Noachian outcrops present felsic rocks, while Hesperian and Amazonian domains seem exclusively basaltic and LCP poor.

3. Martian meteorites

To date, Martian meteorites are the only available petrographic samples which enable constraining the composition of Martian surface and interior, and this will continue so till the Mars Sample Return Mission from Jezero crater scheduled for 2028–2030 [Haltigin et al., 2018].

At the time of writing, a set of 252 Martian meteorites has been found and includes igneous rocks (including pairs) and one breccia (http://www.imca.CC/mars/martian-meteorites.htm,Udryetal2020).
Oxygen isotope measurements revealed that Martian meteorites share a common mass fractionation trend [Clayton and Mayeda, 1996, 1983], indicating an origin from the same planetary body. The definitive link with Mars was made from the isotopic composition of trapped atmospheric gases extracted from shock melt pockets within meteorites that were

identical to the Martian atmospheric composition measured by Viking landers [Bogard and Johnson, 1983]. Martian meteorites offer a unique opportunity to study a large number of surface or subsurface localities compared to the three landing sites analyzed by rover missions (see Figure 1a). Cosmic ray exposures indicating the ejection age of rocks [Eugster et al., 2002] nevertheless revealed that the 252 meteorites sampled just a few locations on Mars, up to ~11 only [Udry et al., 2020]. Martian samples are thus representatively limited but are nevertheless extremely valuable, offering a unique opportunity to thoroughly study a number of surface and subsurface localities, in Earth-based state-of-the-art laboratories that provide high precision—petrological, mineralogical, and geochemical data, unobtainable by landed and orbital spacecraft instruments [McSween et al., 2009]). Martian meteorites are divided into several groups that are described in the following paragraphs.

3.1. *Shergottite–Nakhlite–Chassignite*

Most Martian meteorites, the so-called SNC, are divided into three main groups shergottite, nakhlite, and chassignite representing respectively 82%, 14%, and 3% of all Martian meteorites (https://www.imca.CC/mars/martian-meteorites.htm). Such an apparent diversity actually hides first order common features. A vast majority of SNC contain abundant, often coarse-grained, pyroxene and olivine grains compared to the low amounts of maskylenite (shocked amorphous feldspar crystals), which represent less than 25% of the rock. In other words, Martian meteorites essentially come from mafic and ultramafic cumulates that crystallized at depth. SNC composition thus corresponds to depleted-alkali basalts in the Total Alkali Silica (TAS) diagram (Figure 5).

Shergottites, which are the dominant group, are further subdivided into basaltic, picritic, and lherzolitic shergottites. Among the basaltic subgroup, most meteorites are coarse-textured with high pyroxene/maskelynite ratio (i.e. superchondritic CaO/Al_2O_3 ratio) and are merely represented by mafic to ultramafic cumulates resulting from the fractionation of basaltic liquid at depth. Note that only few basaltic shergottites have a true basaltic cotectic composition (QUE 94201, EET790001, NWA, Los Angeles, NWA 8159). Picritic shergottite subgroup containing up to 7–29% olivine phenocrysts tends to be less affected by crystal accumulation processes and thus is closer in texture to olivine basalt [Gross et al., 2011]. Lherzolitic shergottites are olivine–pyroxene ultramafic cumulates. Collectively, the whole set of shergottites is young, dated at 0.16 to 2.4 Gyr i.e. late Amazonian [Lapen et al., 2017, Nyquist et al., 2001, and reference therein].

Nakhlites and chassignites are clinopyroxene–olivine-rich cumulates sharing common features, such as a ~1.3 Ga Amazonian crystallization age and an ejection age of 11.8 Ma, suggesting that they were part of the same hypabyssal intrusions or thick lava flows or sills [Nyquist et al., 2001, Udry et al., 2020]. Melt inclusions within cumulus olivine of chassignites are sometimes evolved with alkaline compositions [Nekvasil et al., 2007].

Although shergottites provide isotope anomalies of importance for the pre-Noachian global scale differentiation timing, i.e., core–mantle differentiation and primary crust formation [Dauphas and Pourmand, 2011, Debaille et al., 2009, Elkins-Tanton et al., 2005], these young volcanic SNC meteorites do not provide any direct insights into the petrography of the early Noachian crust. Only two specimens out of 252 Martian meteorites, of early Noachian age, might tell us more about the nature of the early Martian crust: an orthopyroxenite and a regolithic breccia.

3.2. *The orthopyroxenite Allan Hills 84001*

The Allan Hills (ALH 84001) meteorite found in Antarctica, is a coarse-grained cataclastic orthopyroxenite cumulate of its own group that was added to the SNC classification [Mittlefehldt, 1994, Thomas-Keprta et al., 2009]. ALH84001 has been dated to be from Noachian, revised from 4.5 Gyr to 4.091 ± 0.03 Ga according to Lu–Hf isotope data [Lapen et al., 2010]. This age is consistent with 4.074 Ga obtained by Pb isotopes [Bouvier et al., 2009, Lapen et al., 2010]. The meteorite contains 97% orthopyroxene crystals ($En_{70}Fs_{27}Wo_3$), 2% chromite, 1% maskelynite ($An_{35}Ab_{62}Or_3$), and 0.15% phosphate with minor augite, olivine, and secondary Fe–Mg–Ca carbonates [Mittlefehldt, 1994]. Its cumulate nature and its mineralogy homogenized by sub-solidus diffusion processes make the bulk rock composition to shift

from that of the parental melt because of crystal accumulation. This meteorite is thus of complex use for the reconstruction of magmatic process on early Mars although the parental melt of ALH 84001 might share some affinities with that of shergottites [Barrat and Bollinger, 2010].

3.3. *The regolithic Martian breccia*

The Martian breccia NWA 7034 and its paired stones (7533/7475/7906/7907/8114/8171/8674/10922/Rabt Sbayta 003) are of exceptional interest to study the early Martian crust [Agee et al., 2013, Humayun et al., 2013, Wittmann et al., 2015]. To cite Agee et al. [2013], "NWA 7034 is not just one rock, but it is like a geological field area conveniently aggregated in one rock". The NWA 7034 and paired meteorites are the first indurated polymict breccia from Mars that could be representative of the craterized ancient surface of the southern hemisphere [Wittmann et al., 2015]. Zircon grains found within some lithic clasts have been dated to be ~4.47 Ga old, making them one of the oldest fragments currently described from Mars [Humayun et al., 2013, Nyquist et al., 2016]. The breccia provides unique insights into the nature of the primitive crust and early magmatism on Mars. It is formed by a mixing of effusive and extrusive igneous polymineralic coarse-grained clasts, including felsic and mafic clasts, monomineralic fragments up to 2 mm size (mainly pyroxenes and feldspars), volcanic deposits, and clast-laden impact melts embedded in a fine-grained crystalline matrix [Agee et al., 2013, Hewins et al., 2017, Humayun et al., 2013, McCubbin et al., 2016a, Nyquist et al., 2016, Santos et al., 2015, Wittmann et al., 2015]. Each of those components is described below.

3.3.1. *The breccia components*

The most striking feature of the breccia observed for the first time in a Martian meteorite is the presence of 4.47 Ga leucocratic felsic igneous clasts embedded in a dark recrystallized clastic groundmass, contrasting with all the young SNC (Figure 4a hand specimen, 4b, c polished section). Described as trachy-andesites, trachytes, and monzonites, felsic clasts are alkaline and represent between 0.14 and 0.28% of the breccia sections [Agee et al., 2013, Hewins et al., 2017, Humayun et al., 2013, Santos et al., 2015, Wittmann et al., 2015]. They are mainly formed by feldspars including andesine and alkali feldspar such as perthitic orthoclase (Or_{88} and antiperthite) and Na-rich plagioclase ($Ab_{70–90}$), pyroxenes like pigeonite, enstatite, augite ($En_{33}Wo_{47}Fs_{20}$), and sometimes diopside. Euhedral chlorapatite is abundant. Zircon and Ti-bearing spinel grains are accessory phases. If most clasts contain anhedral augite partly molden around felspar grains, there are also stringy augite grains with subophitic to alkali feldspar laths. Felsic clast composition is elevated in lithophile incompatible elements in comparison with all other Martian meteorites, which typically contain less than 0.3 wt% K_20 and ~0.6 ppm Th (Table 2, K_2O > 5.6 wt%, Rb > 326 ppm, Ba > 345 ppm, and Th up to 28 ppm [Humayun et al., 2013, Taylor and McLennan, 2009, http://www.imca.CC/mars/martian-meteorites.htm].
This is also true when compared to the Martian crustal average (K_2O = 0.45 wt%, Rb = 12.5 ppm, Ba = 55 ppm, and Th = 0.7 ppm): see Table 2; Figure 5; [Taylor and McLennan, 2009], suggesting that they were formed by crystallization of an evolved melt.

Mafic clasts are norites, microbasalts, and basaltic andesites. Noritic clasts contain orthopyroxene including inverted pigeonite, augite, plagioclase (An ~ 50–30), rare alkali feldspar, Cr-bearing spinel and small amounts of chlorapatite and zircon [Agee et al., 2013, Hewins et al., 2017, Humayun et al., 2013, Santos et al., 2015, Wittmann et al., 2015]. Orthopyroxene crystals are mostly $En_{74–44}Fs_{24–54}Wo_{2–3}$, similar to the cumulate crystal analyzed within the orthopyroxenite ALH84001 [Hewins et al., 2017]. Augite grains coexisting with orthopyroxene equilibrated at temperature of 800–900 °C. Although basaltic clast compositions are characteristic of mafic rocks (SiO_2 < 49.5 wt%, Table 2), Na_2O contents are higher than the average crustal composition, and MgO concentrations are mostly lower (Table 2; Figure 5). On the whole, a vast majority of the lithic clasts found in the meteoritic breccia covers the alkali field in the TAS diagram from basaltic to trachytic end-members (Figure 5).

Monomineralic fragments (up to 2 mm) embedded within the matrix of the breccia are essentially plagioclase ($An_{50–30}$), with small domains of exsolved K-feldspar, and magnesian orthopyroxene ($En_{80–73}$), as well as magnetite–chromite and chlorapatite. All of these clasts and fragments are embedded in a

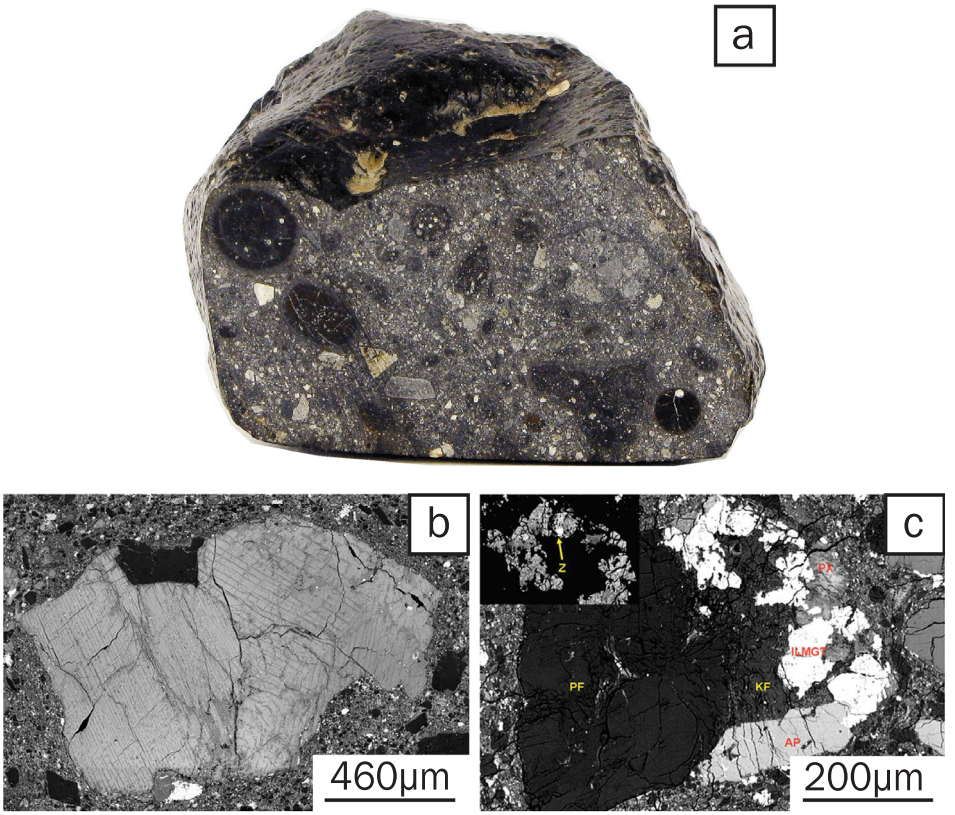

Figure 4. Images of the Martian breccia. (a) Picture of the 4.6× enlarged interior hand specimen of NWA 7475 (image courtesy of Luc Labenne). Numerous light colored felspathic lithic fragments and dark melt spherules are visible in this section. (b) Backscattered electron (BSE) image of noritic clast 7533-5B from NWA 7533 breccia with large piegonite clasts (light gray) and exsolution lamellae associated with andesine crystals (black rectangular shape) within the fine-grained matrix (from Hewins et al. [2017]). (c) BSE image of a large monzonitic clast 7533-4Z from NWA 7533 breccia (from Hewins et al. [2017]).

crystalline and annealed inter-clast matrix, mainly composed of micron-sized plagioclase feldspar grains, with micro- and nano- granular pyroxene crystals. It is of importance to note that except for one olivine, no others have been found within the breccia, as opposed to a majority of SNC meteorites where olivine is ubiquitous. Although most of monomineralic compositions are similar to those of minerals contained within noritic–monzonitic clasts, composition of orthopyroxene extends to more magnesian compositions. Because they are never associated with plagioclase, monomineralic orthopyroxene has been assumed to originate from an orthopyroxenite rock. Interestingly, the orthopyroxene compositions are similar to those of ALH 84001 cumulate crystals [Mittlefehldt, 1994] and are isotopically enriched as well [Lapen et al., 2010].

3.3.2. *Formation mechanisms of the lithic clasts*

High nickel content and high PGE concentrations measured in the breccia suggest the contribution of at least 5–15% of a chondritic impactor [Deng et al., 2020, Humayun et al., 2013]. The large development of exsolution features in coarse crystals in noritic and monzonitic fragments or in mineral clasts, point to slow cooling potentially with a deep-seated plutonic origin, compared to the microbasaltic clasts that likely formed shortly afterward. Therefore, the Martian breccia is thought to be representative of a reworked Noachian regolith, possibly excavated by

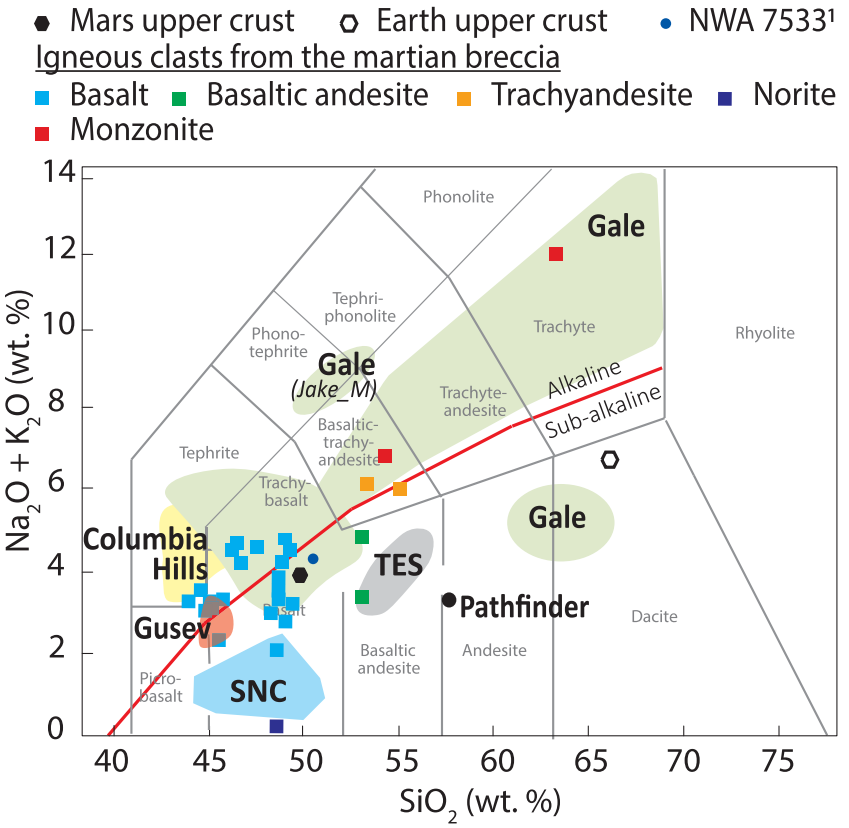

Figure 5. Total alkali content versus silica content adapted from Sautter et al. [2016] allowing geochemical classification of Martian meteorites and rocks analyzed in situ in Ares Vallis (Pathfinder), Gusev plain, Columbia Hills, and Gale crater. [1]Refers to the bulk composition of NWA 7533 from Humayun et al. [2013].

several deep impact melt sheets generated by chondritic impactor(s) [Hewins et al., 2017]. The age of 4.43 Ga of five out of ten zircons found within the noritic–monzonitic fragments indicate a common origin by differentiation of a re-melted primary Martian crust within a large impact melt sheet 100 Myr after the Solar System formation [Hewins et al., 2017]. The age of these zircon grains is strikingly similar to the age of the earliest terrestrial [Valley et al., 2001, Wilde et al., 2001] and lunar zircons [Nemchin et al., 2009], suggesting a coeval crust formation on Earth, Moon, and Mars. Zircon grains analyzed in some of the 4.35 Ga trachy-andesitic clasts [Tartèse et al., 2014] crystallized under oxidizing conditions similarly to magmas that formed the terrestrial crust during the Hadean epoch, pointing to a complex Noachian crust and another similarity with the Hadean terrestrial crust.

To summarize, the early Noachian Martian breccia supports the existence of several ancient melts that formed in the southern highlands by impacts on a primordial crust somewhat differentiated and more or less weathered, 100 Myr after solar system foormation [Hewins et al., 2017]. These impacts generated deep alkali-rich melts where fractional crystallization produced noritic rocks at the bottom and alkali-rich monzonitic rocks in the upper part (Figure 6). These new data from the polymict breccia support an early formation of the Martian crust as well as its somewhat alkali-rich nature.

4. Ground data from rover observations

Rovers and landers allow *in situ* measurements of the Martian surface at much higher spatial resolution compared to orbital data. The chemical composition

Table 2. Major and trace element composition of the most representative igneous clasts in the Martian breccia compared to that of the averaged Martian crust

	NWA7533				NWA7034			**NWA 7475**	**NWA 7034**	Average
	Monzonite		Norite	Microbasalt	Basalt-andesite		Trachy-andesite	**Bulk**	**Bulk**	Mars crust
	Clast II	Clast II	Clast IX	Clast VI	Clast 1	Clast 77	Clast 56			
Major elements										
SiO_2	53.0	63.0	48.2	47.6	53.6	53.5	54.50	**48.3**	**47.6**	49.3
TiO_2	0.40	0.20	0.53	1.11	0.70	1.90	1.20	**1.02**	**0.98**	0.98
Al_2O_3	13.6	17.5	0.86	13.7	12.8	16.5	12.30	**10.7**	**11.2**	10.5
FeO_T	8.05	3.60	28.7	13.9	13.2	10.9	12.10	**16.6**	**13**	18.2
MgO	3.60	0.80	15.0	6.59	9.70	2.20	7.41	**10.9**	**7.81**	9.06
CaO	11.4	2.20	5.48	10.6	6.30	10.1	4.27	**7.04**	**8.93**	6.92
Na_2O	1.81	5.00	0.13	4.36	3.20	4.60	3.27	**2.8**	**3.74**	2.97
K_2O	5.58	7.20	0.21	0.32	0.2	0.40	2.79	**0.47**	**0.34**	0.45
Total	97.4	99.5	99.10	98.20	99.7	100.1	97.90	**97.8**	**93.6**	98.4
Trace elements										
Rb	327	387	12.3	4.60	—	—	—	**—**	**17.1**	12.5
Sr	142	105	6.00	181	—	—	—	**—**	**115**	—
Th	28.5	1.19	0.18	0.92	—	—	—	**—**	**2.64**	0.70
Ba	644	345	47.0	89.0	—	—	—	**—**	**—**	55.0

Major element composition are in wt% and trace elements are in ppm.

"—" corresponds to the absence of any data.

Compositions of clasts within NWA 7533 are from Humayun et al. [2013], and those in NWA 7034 are from Santos et al. [2015].

Bulk composition of NWA 7475 and NWA 7034 are from Wittmann et al. [2015] and Agee et al. [2013], respectively.

The average Martian crust composition is from Taylor and McLennan [2009].

and mineralogy of the Martian surface obtained from ground analyses provide ground truth for orbital experiments and allow a certain group of meteorites found on Earth to be linked to Mars. Each landing site is unique and contributes to our understanding of the diversity of Martian rocks and the wide range of geological processes that generated them. Over time, rover and lander payloads have become increasingly sophisticated, improving their ability to characterize rock texture, mineralogy, and geochemistry at hand specimen scale. The Alpha Particle X-ray spectrometer (APXS), which had been onboard all the rovers since the earliest mission in 1997, measures the elemental whole-rock composition of ~1.7 cm diameter spots on rock surface [Gellert et al., 2013, and references therein]. As an example of sophisticated instruments onboard the most recent rover (Mars Science Laboratory *Curiosity* rover, 2012), the ChemCam laser-induced breakdown spectrometer (LIBS) is the first laser sent to Mars, which allows to measure the composition of rocks located at distance from the rover, without the necessity of rock contact [Maurice et al., 2012, Wiens et al., 2012]. The CheMin instrument analyzes the mineralogy of drilled rocks using X-ray diffraction [XRD; Blake et al., 2012]. The Mars Hand Lens Imager (MAHLI) is the most resolved imager ever made for a Martian mission.

Since 1997, four missions have landed thousands of kilometers away from each other in equatorial regions of Mars (Figure 1): Mars *Pathfinder* in 1997, the Mars exploration rovers (MER) *Spirit* and *Opportunity* in 2004, and *Curiosity* since 2012 (Figure 1). Three of them allow the analysis of Noachian/early Hesperian terrains on Mars, providing new insights into the early Martian crust that is coeval with Archean cratons on Earth: *Pathfinder* rover, which

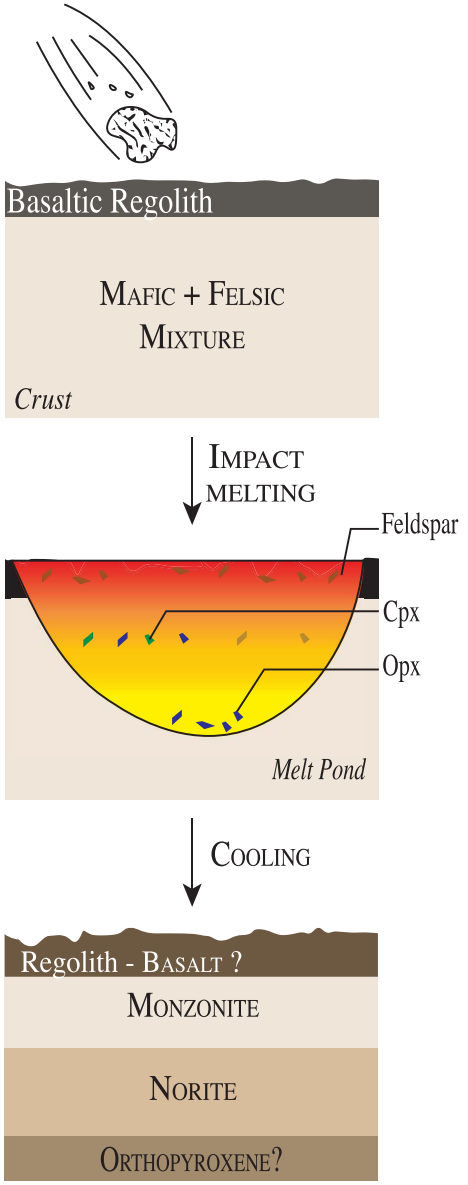

Figure 6. Sketch of the formation of igneous clasts within the Martian breccia (adapted from Hewins et al. [2017]).

landed in *Ares Vallis*; the *Spirit* rover in *Gusev crater*; and *Curiosity* in *Gale crater* (Figure 1).

In *Ares Vallis* (Figure 1a,b), *Pathfinder* traveled within the mouth of a large outflow channel located on *the south of Chryse Planitia,* where debris washed down from the southern hemisphere was concentrated [McSween et al., 1999, and references therein], thus sampling a variety of rocks originating from a small area including fragments of the Noachian crust. The APXS instrument onboard the lander analyzed five Si-rich and alkali-poor (SiO_2 ~ 57.7 ± 1.7 wt%; $Na_2O + K_2O$ ~ 5.3 ± 0.7 wt%) igneous rocks identified as andesites, which likely formed between late Noachian and early Hesperian [Foley et al., 2003, McSween et al., 1999]. The andesitc interpretation is still questioned because of the absence of sophisticated imager and tools that could identify minerals within rocks. The compositions of the five rocks can be either explained by crystallization of an evolved primary melt or by alteration processes in acidic conditions [Foley et al., 2003, McSween et al., 1999]. No consensus has been reached.

Gusev crater, where the *Spirit* rover landed in 2004, is located in the *Aeolis region* along the dichotomy boundary at the northern edge of the highly cratered Noachian southern highlands and south of the Medusae fosse formation (Figure 1a,b). The crater floor is covered by a Hesperian basaltic flow [~3.65 Gyr; Greeley et al., 2005] containing prominent olivine phenocrysts (Adirondack class) with Mg# > 0.5 comparable to olivine-phyric shergottites (see Section 3.1). The volcanic flow embays terrains of the *Columbia Hills*, a series of elevated outcrops distinctive from the rocks of the crater floor. The field relationship between the base of the Columbia Hills stratigraphic sequence and the crater floor itself is still unclear. Columbia Hills could either represent a central uplift of older Noachian crater floor [McCoy et al., 2008] or post-date the crater formation and its filling by Hesperian olivine basalt lava flow [Arvidson et al., 2006]. The volcanic flows at Columbia Hills were identified as the first alkali-basalt lithologies described on Mars (e.g. Wishstone, Backstay, and Irvine Figure 5). These alkali-rich rocks range from aphanitic basalts (Irvine-class dyke) and trachy-basalts (Backstay float) to blocks of tuff, i.e. plagioclase-bearing pyroclastic rocks or impact ejecta that have experienced moderate alteration (Wishstone class, [Ruff et al., 2006]). Irvine, Backstay, and Wishstone are likely weakly affected by secondary processes and are usually referred to as alkaline volcanic rocks or alkali-basalts [McSween et al., 2006a]. They are aphanitic rocks that likely contain olivine and pyroxene and have Na_2O + K_2O ranging from 3 wt% to 5.5 wt% and SiO_2 contents <52 wt% [Arvidson et al., 2008, Ming et al., 2008]. They still present a significant chemical diver-

sity. Irvine is a sub-alkaline basalt that is similar to Adirondack-class basalts with much higher K_2O concentrations, slightly higher Na_2O, and lower CaO and Al_2O_3. In contrast to Irvine, Backstay contains more elevated Al_2O_3 contents and has a higher Mg# (53.3) than Adirondak-class basalts (50.1), Irvine (46.2), and Humboldt Peak basalt (49.7). The Wishstone class basalts are part of the Watchtower stratified outcrop and present tephritic composition, with Na_2O + K_2O ranging from 1.5 to 5.5 wt% and SiO_2 contents <52 wt% [Arvidson et al., 2008, Ming et al., 2008]. These mafic rocks extended the compositional range of igneous rocks encountered on Mars to the alkaline domain. Although not visually identified [McSween et al., 2006a, Squyres et al., 2007, 2006], normative andesine–oligoclase values in Columbia Hills rocks range up to ~55% and several rocks such as Backstay contain up to 7% of normative K-feldspar [Ming et al., 2006], which is consistent with the strong plagioclase signature in Mini-TES spectra observed in Wishstone [Squyres et al., 2006].

Gale crater, where the *Curiosity* rover landed in 2012, is located as well in the **Aeolis region** along the dichotomy boundary (Figure 1a,b). The crater, 155 km in diameter, was formed by an impact in early Hesperian time within a 4.21 Gyr old basement [Le Deit et al., 2013, Farley et al., 2014]. The Mars Science Laboratory (MSL) mission is the first mission to probe such ancient terrains (~early Noachian). The analyses of 180 igneous rocks along *Curiosity*'s 20 km traverse makes *Gale crater* the most thoroughly documented Noachian igneous terrains on Mars [Cousin et al., 2017]. Broadly speaking, magmatic materials were found either as float rocks (loose boulders) scattered on a sedimentary unit characterized by discontinuous sandstones at the foot of an alluvial fan, or as large rounded clasts within conglomerates. Floats, which could result from the disaggregation of conglomerates, are interpreted to have originated from a subsurface magmatic sequence exposed in the northern crater wall. Transportation through stream water would have deposited the floats on the crater floor, at the end of an alluvial fan. No magmatic outcrop has been detected from orbit within the crater wall or outside the crater, suggesting that it now is buried beneath a basaltic regolith [Sautter et al., 2015]. Onboard the rover, the Chemistry Camera instrument (ChemCam) identified a large diversity of float igneous rocky blocks using a highly resolved remote micro imager (RMI) enabling textural characterization, and a laser-induced breakdown spectroscopy (LIBS), which allows chemical analyses at a micrometric scale (laser spot diameter: 350–550 μm). The floats and clasts range from darkish and grayish mafic rocks to unexpected light-toned felsic igneous rocks [Sautter et al., 2014, 2015, 2016, Cousin et al., 2017]. Overall, volcanic rocks discovered in Gale crater highlight an extensive compositional diversity. Two magmatic suites including five groups of rocks [Cousin et al., 2017] have been identified: an alkaline trend with basalts and basanites, gabbros and norites, trachy-andesites, mugearites, and trachytes, and a sub-alkaline trend including plutonic rocks such as diorites and quartzo-diorites (Figures 5–7). Interestingly, the coarse-grained component of the soils analyzed in the vicinity of the igneous materials is also felsic in composition [Meslin et al., 2013] providing supporting evidence for local felsic bedrock. For the purpose of the present paper, we will focus on alkaline effusive rocks, i.e., the basalt, trachy-basalt, trachy-andesite, and trachyte sequence (Figure 7). Numerous rocks within this sequence show extreme contents of alkali elements, especially for potassium. Representative compositions of one igneous rock from each described group are summarized in Table 3 and shown in the TAS diagram in Figure 5.

Basalts correspond to dark-toned rocks with aphanitic textures showing local conchoidal fractures (Figure 7a). Most individual crystals are indistinguishable, and most basalts contain feldspar microliths, which are smaller than the ChemCam laser beam (≪350 μm). The dark groundmass is dominated by Mg-pigeonite (the so-called LCP). In contrast to the olivine phenocrysts described in Adirondack-class basalts from Gusev crater, olivine crystals have never been observed in the Gale dark rocks. The lack of olivine is explained by the whole-rock composition showing that basalts and basanites are Fe rich with a large range of low Mg number (Mg#, $0.15 < Mg\# < 0.5$) in comparison with previous rover and lander missions ($Mg\# > 0.5$) [Cousin et al., 2017, McSween et al., 2006b, Squyres et al., 2006].

Jake Matejevic (Jake_M), analyzed by both the APXS and the ChemCam instruments, was described as the first Martian mugearite [Stolper et al., 2013]. Dark gray in color, it has a basaltic composition that is highly alkali-rich (up to 7 wt% Na_2O and

Table 3. Composition of representative rocks for each igneous group identified in Gale crater compared to the Martian average crust for reference

	Basalt Gunflint	Trachy-basalt HarrisonC1	Trachyte Meeting_House	Gabbro La_Reine	Diorite Noriss2	*Average Mars Crust*
Major elements						
SiO_2	48.4	57.0	65.0	50.30	57.8	*49.3*
TiO_2	1.41	0.62	0.90	0.92	1.08	*0.98*
Al_2O_3	7.92	19.4	15.4	11.2	18.2	*10.5*
FeO_T	22.6	6.59	5.34	16.8	8.48	*18.2*
MgO	10.8	1.90	1.71	11.9	1.92	*9.06*
CaO	5.17	1.96	2.76	5.73	5.46	*6.92*
Na_2O	2.53	6.08	5.26	2.80	6.18	*2.97*
K_2O	1.17	2.78	3.61	0.30	0.91	*0.45*
Total	100.0	100.0	100.0	100.0	100.0	*98.4*
Trace elements						
Rb	44	93	92	21	81	*12.5*
Sr	48	115	60	34	232	
Ba	49	114	964	87	205	*55*
CIPW norm						
Quartz	—	—	11.9	—	—	
Plagioclase	34.5	58.3	53.1	47.8	68.5	
Orthoclase	8.70	16.0	21.6	2.17	5.20	
Nepheline	—	4.58	—	—	—	
Diopside	15.1	8.88	1.34	8.77	6.50	
Hypersthene	11.4	—	10.8	21.2	11.5	
Olivine	28.6	8.24	—	19.0	2.21	
Ilmenite	1.80	1.14	1.71	1.15	1.98	
Rutile	—	—	—	—	—	
Density	2.84	2.79	2.74	**3.14**	2.84	
Mg #	45.9	36.6	36.0	55.8	28.7	

The composition of these rocks are normed to 100% and are from Cousin et al. [2017]. Major element concentrations are expressed in wt% and trace element contents are in ppm.
CIPW norm in % illustrates the potential mineralogy according to the composition. The occurrence of quartz, feldspars, pyroxenes and oxides are in agreement with single point analyses and imaging observations (see Cousin et al. [2017] for more details).
"—" corresponds to 0%.

2 wt% K_2O, Figure 5), and 16% to 17% normative nepheline. This alkaline rock is fractionated like most of the basaltic rocks encountered in Gale crater, as illustrated by its low MgO contents (MgO = 4.5 wt%). Based on comparison with terrestrial mugearites, [Stolper et al., 2013] interpreted Jake_M as the product of extensive fractional crystallization of an alkali-basaltic liquid. Note that the igneous nature of Jake_M is debated due to its ambiguous texture and composition [e.g., Mangold et al., 2017].

Trachy-basalts/andesites are porphyritic rocks with large feldspar euhedral crystals (up to a few

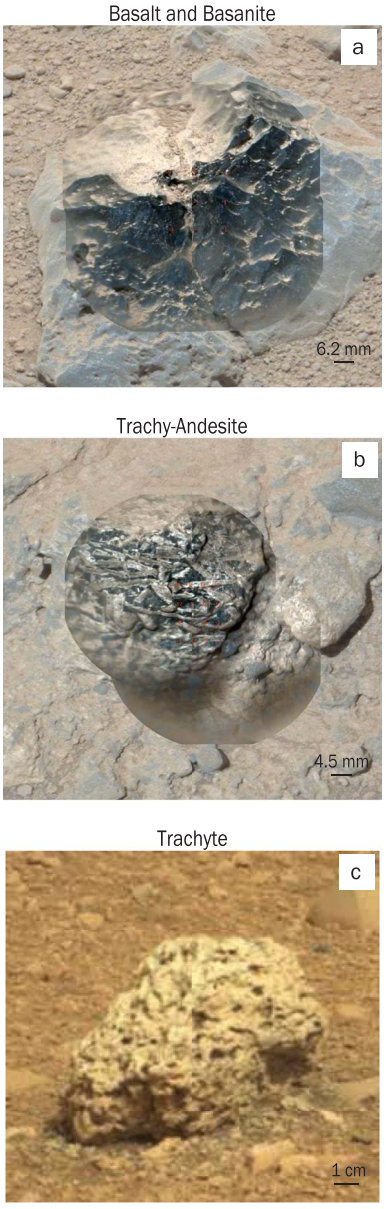

Figure 7. (a–c) RMI images merged with Mastcam images of igneous rocks encountered at Gale crater adapted from Cousin et al. [2017]. From (a) to (c), those rocks are named Pisolet, Harrison, and Becraft.

centimeters) embedded in a dark-gray fine-grained mesostasis with a ferro-augite composition [Figure 7b; Sautter et al., 2015, Cousin et al., 2017]. Feldspar proportion range from 47% to 57% of the rocks, except for one rock named Bindi presenting 80% of coarse feldspar with a typical cumulate texture. Feldspar compositions range from andesine to oligoclase [Cousin et al., 2017, Payré et al., 2020].

Trachytes are leucocratic rocks with almost no visible grains, presenting conchoidal fractures, and having sometimes a vesiculated or pumiceous appearance (Figure 7c). The ground mass is dominated by alkali feldspar compositions, mainly anorthoclase-like and sometimes sanidine-like. Trachyte composition is alkali-rich ($Na_2O \sim 5$ wt% and $K_2O \sim 3.5$ wt%; Figure 5) with a low Mg number (0.3). Felsic rocks, which include trachy-andesites and trachytes, are enhanced in incompatible major and trace elements in comparison with the Martian crustal average (e.g., $0.4 < K_2O < 3.8$ wt%, Rb $\gg$ 50 ppm, Ba $\gg$ 60 ppm [Payré et al., 2017; Table 3].

To summarize, rover exploration allows deciphering two igneous series, a sub-alkaline suite that includes the potential andesites from ***Ares Vallis*** and the quartz-diorites from ***Gale crater*** (Figure 5), and an alkaline suite that comprises the alkaline rocks found in ***Colombia Hills*** and ***Gale crater***. The alkaline olivine-free (Mg-poor) characteristic of effusive rocks at Gale crater is similar to the early Noachian alkaline clasts from the regolithic meteorite and the Wishstone rocks (possibly of Noachian age) analyzed by the *Spirit* rover. All together, the orbital and rover data and the Martian brecciated meteorite analyses, especially of the Noachian effusive rocks in Gale crater and the 4.47 Ga felsic clasts in the Martian breccia, point to diversified, evolved and alkaline rocks produced early in Martian history.

5. Discussion: origin of alkaline magmatism on Mars

Except for the andesitic and dioritic rocks detected by the *Mars Pathfinder* and the *Curiosity* missions, Noachian igneous materials from Mars are grouped into two lithologies: alkaline rocks and orthopyroxenite (LCP)-bearing rocks. The following subsections discuss how such rocks could have been formed.

5.1. *How did alkaline rocks form on Mars?*

Alkaline melts found on Mars can be generated through various mechanisms including (1) low degree of partial melting of a primitive Martian mantle or a metasomatised mantle source, (2) fractional

crystallization of a basaltic liquid in the presence of water or under high pressure conditions that delay the crystallization of plagioclase toward high fractionation degrees, and (3) crustal assimilation of crustal rocks.

(1) Magmas formed by partial melting of the mantle are primary, i.e., largely unaffected by fractional crystallization. In this case, alkali-rich liquids are formed by low degree of partial melting of either a primitive mantle or a regionally K-metasomatized mantle source [Schmidt and McCoy, 2010, Schmidt et al., 2014]. Low degree of partial melting of a primitive fertile mantle (containing <1% garnet) has been suggested from the Martian breccia bulk composition [Humayun et al., 2013, Sautter et al., 2015]. Broadly speaking, Mars is able to generate magmas that are on average richer in alkali content than the Earth because geochemical models predict that bulk silicate Mars contains 30% more elevated Na concentrations and 15% higher K concentrations than bulk silicate Earth [Palme and O'Neill, 2014, Wanke and Dreibus, 1988]. As a result, alkaline magmas should be more common on Mars than they are on Earth, where alkaline lavas represent less than 1 vol.% of terrestrial igneous rocks [Winter et al., 2010]. Based on elevated K/Ti ratio [Filiberto, 2017], mantle metasomatism has been suggested for the generation of some alkali rocks from Gale crater, including Jake_M [Rice et al., 2017, Schmidt and McCoy, 2010, Schmidt et al., 2016, Treiman and Medard, 2016], although the Martian interior is thought to be dry according to low H_2O estimations within the parental melt of Martian meteorites [150–850 ppm; Filiberto et al., 2016, McCubbin et al., 2016b]. Note that water estimates of the mantle are obtained from SNC, which again are young volcanic rocks resulting from melting of a dehydrated mantle that is likely distinct in composition and water content from the primitive mantle [McCubbin et al., 2012].

(2) Fractional crystallization has been suggested to explain the diversity of alkaline igneous materials in Columbia Hills, Gale crater, within the Martian breccia, and chassignites [Roger H Hewins et al., 2017, Nekvasil et al., 2007]. The Columbia Hills alkaline rocks have been interpreted to be formed by fractional crystallization of either a primitive oxidized basaltic magma with Adirondack-like compositions at various pressures [0.1–1 GPa or 10–80 km; McSween et al., 2006a] or primary basaltic liquids produced by various partial melting degrees of the mantle [Schmidt and McCoy, 2010]. If true, alkaline rocks from Columbia Hills would post-date the Adirondack-class basalts located within the Gusev crater floor plains whereas the chronology between Columbia Hills and the Gusev crater floor has not been firmly established [Arvidson et al., 2006, Squyres et al., 2006].

Using pMELTS thermodynamical models Ghiorso et al. [2002], Sautter et al. [2015] showed that basaltic end-members of Gale crater rocks may have first originated by low degree of partial melting (6%) of primitive mantle at pressure 1 GPa (~80 km depth) before undergoing fractional crystallization at a pressure of 1 bar. Running additional thermodynamical models, Udry et al. [2014, 2018] propose that felsic alkaline rocks from Gale crater were produced by fractional crystallization at crustal depths (up to 0.4 GPa or ~35 km) of basaltic liquids containing 0.5 wt% of H_2O. Note that the large andesine and oligoclase phenocrysts within a trachy-andesite (Figure 7b) in Gale crater can also be explained by fractional crystallization at crustal depth (up to 0.4 GPa) of a basaltic liquid with 0.5 wt% of H_2O, which formed by relatively low extent of melting of a primitive mantle composition [Payré et al., 2020]. If igneous, Jake_M in Gale crater likely derived as well from melts that have undergone fractional crystallization at depth (≤0.4 GPa) with or without the presence of water [Stolper et al., 2013, Collinet et al., 2015]. Although fractionation models seem to match the composition and mineralogy of Gale crater alkaline rocks, trachytic liquids would be produced at >60% of fractionation degree, reaching the critical crystallinity that rheologically prevents eruption [Brophy, 1991].

Felsic and alkaline clasts from the breccia have been interpreted to come from fractionation at the top of an evolved impact melt sheet [Figure 6; Hewins et al., 2017, Humayun et al., 2013]. Comparison between experimental works and terrestrial intra-plate rocks suggest that melts trapped into cumulus olivine of several chassignites were similar to alkaline more or less silica-saturated hawaiite, likely produced by hydrous fractional crystallization of a basaltic melt at pressures >0.4 GPa [Nekvasil et al., 2007].

(3) Crustal assimilation is a common process on Earth that can enrich melts in incompatible elements contained within the crust and that can sometimes increase the alkalinity of the liquids [Beard and Lof-

gren, 1991]. According to thermodynamical models, Ostwald et al. [2020] propose that felsic alkaline rocks from Gale crater could be formed by crustal assimilation followed by fractional crystallization of a basaltic liquid at crustal pressures (up to 0.6 GPa or ~50 km) with H_2O = 0–0.5 wt%.

In summary, the Hesperian or Noachian alkaline rocks from Columbia Hills and the Amazonian evolved melts included within olivine cumulus of chassignites were likely produced by fractional crystallization at crustal depths, the Noachian alkaline clasts within the Martian breccia potentially formed by fractionation at the top of an alkaline-rich impact melt sheet of a preexisting alkaline crust that was produced 4.43 Ga ago by low degree of partial melt of a fertile mantle, and the formation of Noachian alkaline rocks from Gale crater remain debated (mantle metasomatism, or fractional crystallization certainly accompanied by crustal assimilation; Figure 1). Note that according to partial melting experiments [Collinet et al., 2015], low extent of melting of a primitive mantle composition cannot reproduce trachy-andesitic and trachytic compositions observed in Gale crater. In any case, alkaline igneous materials from Mars were produced by crustal magmatic processes common on Earth [Basaltic Volcanism Study Project, 1981].

5.2. *How did low calcium pyroxene-rich magmatic rocks form?*

While Hesperian and Amazonian lavas are olivine- and HCP-rich basaltic flows, LCP-rich outcrops are a striking feature of the Noachian magmatism [Baratoux et al., 2013, Mustard et al., 2005, Poulet et al., 2009]. As a reminder, HCP corresponds to augite, diopside, and hedenbergite, while LCP corresponds to pigeonite and orthopyroxene. Noachian LCP-rich rocks can be either effusive (basalts) or plutonic rocks (norites or LCP-rich cumulates). Orbital spectroscopy is unable to distinguish between lithologies due to the lack of close imaging and the identification of a potentially incomplete mineral assemblage. Within the Noachian meteorites, LCP-rich rocks are plutonic: LCP cumulates (ALH 84001 and LCP mineral clasts within the breccia) and noritic clasts within the breccia. In contrast to Noachian LCP-rich rocks, Amazonian SNC meteorites are olivine-rich basalts (olivine-phyric shergottites) and olivine-rich or HCP-rich cumulates (lherzolitic shergottites, nakhlites and chassignites). On the ground, Hesperian lavas at Gusev are olivine-rich basalts, while Gale crater basalts formed in Noachian time are olivine-free and have generally a low non-chondritic Ca/Al ratio. All together, Noachian basaltic rocks are LCP-rich and olivine-free whilst Hesperian to Amazonian cumulate rocks are generally LCP-poor and olivine-rich with the exception of sparse evolved melts observed within Amazonian meteorites (Figure 1).

Assuming that primary unfractionated magmas produced by partial melting of a primitive mantle are the main building blocks of the Martian crust, Baratoux et al. [2013] modeled the transition in pyroxene composition particularly prominent at the Noachian/Hesperian period boundary with LCP/(HCP+LCP) ratio decreasing from 0.4 to 0.2 [Poulet et al., 2009]; and reference therein). Under batch melting conditions, liquids are in thermodynamic equilibrium with the base of the lithosphere and directly ascending to the surface without fractionation. The composition of the primary melts and the crystallization sequence at the surface were calculated for partial melting at different depths (i.e. thickness of the lithosphere which increases from Noachian to more recent time) and different temperatures accounting for cooling of the mantle with time. High degrees of melting lead to a significant contribution of orthopyroxene at shallow depths while melting of olivine is inhibited, favoring the formation of Si-rich liquids in Noachian time compared to Hesperian/Amazonian periods. Overall, high degrees of melting at low pressures favor the crystallization of LCP-rich olivine-poor assemblages within Noachian melts, explaining the lack of olivine in basaltic clasts of the regolithic breccia and in igneous rocks from Gale crater that all formed at lower crustal pressures. Such high degrees of partial melting can be explained as follows. Early in Mars history, the mantle was warmer, thus producing high melting point melts as suggested by Baratoux et al. [2013, 2011]. Mantle plumes, which are thought to have existed in Noachian time [e.g., Citron et al., 2018, Harder and Christensen, 1996], could also contribute to high degree liquids. The lithosphere in Noachian was thinner than later in time. High degrees of partial melting at shallow depths would thus be common in Noachian time.

The orbital observations of large LCP-rich terrains can be explained by (1) the rapid ascent of LCP-rich

liquids produced by high degrees of melting, leading to the formation of vast LCP-rich effusive lavas at the surface of Mars. No fractionation would occur. Another possibility is that (2) LCP-rich liquids are stuck at depths because of a low rate of ascending. In that case, magmas would crystallize, fractionating LCP crystals at the bottom, forming orthopyroxene cumulates, i.e., intrusive rocks, and leaving behind a differentiated alkaline liquid that could erupt and produce feldspar-rich basaltic rocks as observed at Gale crater. Another hypothesis that can be envisioned is (3) heavy bombardment on a LCP-rich crust which was formed by LCP-rich primary magmas formed by high degree of partial melting. The melt sheets induced by wide impacts could fractionate LCP sinking at the bottom leaving behind residual alkaline melts, as suggested by the lithic clasts of the regolithic breccia NWA 7533 and its paired meteorites. The two latter scenarios can explain both LCP cumulates observed within Noachian meteorites, and alkaline olivine-free rocks observed in Gale and Gusev crater. The thickening of the Martian crust and the global cooling of the planet interior likely led in recent times to crystallization events at depth as suggested by the occurrence of evolved melts trapped within some Amazonian chassignites.

Recent results obtained for the past ten years both from spacecraft and meteorite analyses offer exceptional new insights into magmatic processes on early Mars. This extensive data set points to an early magmatic history of Mars considerably more complex than previously acknowledged. The coexistence of alkali rocks and LCP-bearing rocks in the Noachian epoch leaves diverse questions unanswered. Is alkali magmatism coeval with LCP fractionation at depth at a global scale within early Noachian terrains? If so, Noachian LCP-rich areas detected from orbit would likely correspond to cumulate outcrops. Alternatively, LCP-detections from orbit could correspond to LCP-rich lava flows (unfractionated liquid migrating to the surface).

5.3. *Alkaline magmatism in a stagnant lid system*

Mars is considered as a stagnant lid system as no apparent plate tectonics has been observed. Volcanism on Mars can be thus be considered as analogous to terrestrial intra-plate magmatism and oceanic hotspot volcanism. In such settings, alkaline volcanism is common on Earth, although representing <1 vol.% of terrestrial rocks [Winter et al., 2010]. High pressure of melting (>1 GPa), metasomatism, low degree of partial melting, and fractional crystallization of mantle-derived magmas lead to the formation of alkaline rocks on Earth as observed for example in the Terceira island in Azores [Nekvasil et al., 2000] and the Ngatutura basalts in New Zealand [Briggs et al., 1990]. Such formation contexts are consistent with the generation of alkaline rocks on Mars, as discussed in Section 5.1. According to geochemical models, the terrestrial bulk silicate contains 30% less Na concentrations and 15% lower K concentrations than the Martian bulk silicate [Palme and O'Neill, 2014, Wanke and Dreibus, 1988]. Hence, Martian magmas derived from the mantle should be on average richer in alkali contents than the Earth. This is consistent with the average crust being formed by relatively low extent of melting (10%), which favors the accumulation of alkali as suggested by [Kiefer, 2003], and the high amount of radioactive elements like K in the southern hemisphere [Thiriet et al., 2018]. Yet, only a few locations on Mars present alkaline igneous rocks, suggesting that they might be hidden under subsequent late Noachian to Hesperian and Amazonian basaltic materials observed at the surface of Mars from orbit. Interestingly, most alkaline rocks discovered from Mars are felsic, meaning that felsic alkaline rocks are likely buried under a few meters of basaltic flows. The topographic-geoid ratio derived from geophysical data obtained from orbit supports the existence of light differentiated crustal components underneath heavy basaltic rocks [Baratoux et al., 2014]. The occurrence of a large amount of buried alkaline differentiated rocks can explain such observation, implying that the vast majority of the Martian data set might be biased: young SNC sampling localized regions and rover and orbital data mainly measuring young surface basaltic components (≫3.7 Ga). If true, the Martian crust would be extremely complex, with potential orthopyroxene cumulates at the bottom, alkaline felsic components at the upper part, and a homogeneous basaltic cover on the top. Note that isotopic analyses of zircons from the meteorite breccia reveal an enriched basaltic or andesitic crust extracted as soon as 20 Myr after the solar system formation [Bouvier et al., 2018], i.e., coeval to the terrestrial primordial crust forma-

tion [Elkins-Tanton, 2008, Valley et al., 2014]. Fractional crystallization and assimilation of such a crust would lead to alkaline felsic components, especially with a supply of alkali elements within the crust from mantle-derived melts.

Alkaline felsic magmatism discovered on Mars is mostly ancient, >3.7 Ga, and zircon grains found in felsic clasts of NWA 7034 are as old as the most ancient zircons ever dated on Earth [>4.4 Ga; Valley et al., 2014]. Terrestrial zircons are the oldest fragments of our planet, and no rock witnessing the magmatic history of Hadean time exists, mainly because of an efficient plate tectonic system that started early in the terrestrial history [e.g., Kamber et al., 2005, Marchi et al., 2014]. With its stagnant lid, Mars preserved such ancient rocks, and the contemporaneous age of Martian and terrestrial zircons and crust formation suggest a similar magmatism on early Earth and Mars.

6. Conclusion

While terrestrial plate tectonics and significant volcanism have erased the first continental crust on Earth, numerous impact bombardments and extensive basaltic volcanism have likely buried a differentiated crust on Mars. Scattered portions of the early Noachian to Noachian crust can still be observed in several excavations and crater walls in the southern hemisphere, as analyzed in Gale crater and other locations as inferred from orbital data. This is precisely the intensity of bombardment on early Mars that might have generalized melt sheets on surfaces initially covered by LCP-rich lava flows formed by melting of hot mantle beneath a thin primordial crust. Fractionation of those melt sheets would favor the fractionation of LCP cumulates at the bottom and alkali residual melts close to the surface, as suggested by the lithic clasts of the regolithic Martian meteorites. Fractionation at crustal depths of LCP-rich primary liquids produced by high extent of melting of the mantle would also lead to the formation of LCP at depths, later forming LCP cumulates similar to the orthopyroxenite ALH 84001, leaving alkaline residual melts that would erupt at the surface of Mars forming alkaline rocks as those observed in Gale crater. The *Insight* mission that landed on Mars in November 2019 has the first successful onboard seismometer (SEIS) ever sent to Mars [Lognonné et al., 2019]. Probing for the Martian interior, especially the deep crust, seismic data should be able to identify putative deep vertical crustal stratification inferred from surfaces analyses. At Jezero crater, the Mars 2020 *Perseverance* mission probes terrains even older than those of previous ground missions. With a cashing system onboard, the *Perseverance* rover is the first of its kind to prepare future Mars sample missions that will likely bring back critical data in terms of Mars' ancient evolved magmatism and its age, providing powerful key information regarding the volcanic history on primitive Earth.

References

Agee, C. B., Wilson, N. V., McCubbin, F. M., Ziegler, K., Polyak, V. J., Sharp, Z. D., Asmerom, Y., Nunn, M. H., Shaheen, R., Thiemens, M. H., Steele, A., Fogel, M. L., Bowden, R., Glamoclija, M., Zhang, Z., and Elardo, S. M. (2013). Unique meteorite from early Amazonian Mars: Water-Rich basaltic breccia Northwest Africa 7034. *Science*, 339, 780–785.

Arvidson, R. E., Ruff, S. W., Morris, R. V., Ming, D. W., Crumpler, L. S., Yen, A. S., Squyres, S. W., Sullivan, R. J., Bell, J. F., Cabrol, N. A., Clark, B. C., Farrand, W. H., Gellert, R., Greenberger, R., Grant, J. A., Guinness, E. A., Herkenhoff, K. E., Hurowitz, J. A., Johnson, J. R., Klingelhöfer, G., Lewis, K. W., Li, R., McCoy, T. J., Moersch, J., McSween, H. Y., Murchie, S. L., Schmidt, M., Schröder, C., Wang, A., Wiseman, S., Madsen, M. B., Goetz, W., and McLennan, S. (2008). Spirit Mars rover mission to the Columbia Hills, gusev crater: mission overview and selected results from the Cumberland Ridge to home plate. *J. Geophys. Res.*, 113, article no. E12833.

Arvidson, R. E., Squyres, S. W., Anderson, R. C., Bell, J. F., Blaney, D., Brückner, J., Cabrol, N. A., Calvin, W. M., Carr, M. H., Christensen, P. R., Clark, B. C., Crumpler, L., Des Marais, D. J., de Souza, P. A., d'Uston, C., Economou, T., Farmer, J., Farrand, W. H., Folkner, W., Golombek, M., Gorevan, S., Grant, J. A., Greeley, R., Grotzinger, J., Guinness, E., Hahn, B. C., Haskin, L., Herkenhoff, K. E., Hurowitz, J. A., Hviid, S., Johnson, J. R., Klingelhöfer, G., Knoll, A. H., Landis, G., Leff, C., Lemmon, M., Li, R., Madsen, M. B., Malin, M. C., McLennan, S. M., McSween, H. Y., Ming, D. W., Moersch, J., Morris, R. V., Parker, T., Rice, J. W., Richter, L., Rieder, R., Rodionov, D. S., Schröder, C., Sims, M.,

Smith, M., Smith, P., Soderblom, L. A., Sullivan, R., Thompson, S. D., Tosca, N. J., Wang, A., Wänke, H., Ward, J., Wdowiak, T., Wolff, M., and Yen, A. (2006). Overview of the spirit Mars exploration rover mission to gusev crater: landing site to backstay rock in the Columbia Hills. *J. Geophys. Res.*, 111, article no. E02S01.

Bandfield, J. L. (2002). Global mineral distributions on Mars. *J. Geophys. Res.*, 107, article no. 5042.

Baratoux, D., Samuel, H., Michaut, C., Toplis, M. J., Monnereau, M., Wieczorek, M., Garcia, R., and Kurita, K. (2014). Petrological constraints on the density of the Martian crust. *J. Geophys. Res.*, 119, 1707–1727.

Baratoux, D., Toplis, M. J., Monnereau, M., and Gasnault, O. (2011). Thermal history of Mars inferred from orbital geochemistry of volcanic provinces. *Nature*, 472, 338–341.

Baratoux, D., Toplis, M. J., Monnereau, M., and Sautter, V. (2013). The petrological expression of early Mars volcanism. *J. Geophys. Res.*, 118, 59–64.

Barrat, J.-A. and Bollinger, C. (2010). Geochemistry of the Martian meteorite ALH 84001, revisited. *Meteorit. Planet. Sci.*, 45, 495–512.

Basaltic Volcanism Study Project (1981). *Basaltic Volcanism on the Terrestrial Planets*. Pergamon Press, New York.

Beard, J. S. and Lofgren, G. E. (1991). Dehydration melting and water-saturated melting of basaltic and andesitic greenstones and amphibolites at 1, 3, and 6.9 kb. *J. Petrol.*, 32, 365–401.

Bibring, J.-P. (2005). Mars surface diversity as revealed by the OMEGA/Mars express observations. *Science*, 307, 1576–1581.

Blake, D., Vaniman, D., Achilles, C., Anderson, R., Bish, D., Bristow, T., Chen, C., Chipera, S., Crisp, J., Des Marais, D., Downs, R. T., Farmer, J., Feldman, S., Fonda, M., Gailhanou, M., Ma, H., Ming, D. W., Morris, R. V., Sarrazin, P., Stolper, E., Treiman, A., and Yen, A. (2012). Characterization and calibration of the chemin mineralogical instrument on Mars science laboratory. *Space Sci. Rev.*, 170, 341–399.

Bogard, D. D. and Johnson, P. (1983). Martian gases in an antarctic meteorite? *Science*, 221, 651–654.

Bouley, S., Keane, J. T., Baratoux, D., Langlais, B., Matsuyama, I., Costard, F., Hewins, R., Payré, V., Sautter, V., Séjourné, A., Vanderhaeghe, O., and Zanda, B. (2020). A thick crustal block revealed by reconstructions of early Mars highlands. *Nat. Geosci.*, 13, 1–5.

Bouvier, A., Blichert-Toft, J., and Albarède, F. (2009). Martian meteorite chronology and the evolution of the interior of Mars. *Earth Planet. Sci. Lett.*, 280, 285–295.

Bouvier, L. C., Costa, M. M., Connelly, J. N., Jensen, N. K., Wielandt, D., Storey, M., Nemchin, A. A., Whitehouse, M. J., Snape, J. F., Bellucci, J. J., Moynier, F., Agranier, A., Gueguen, B., Schönbächler, M., and Bizzarro, M. (2018). Evidence for extremely rapid magma ocean crystallization and crust formation on Mars. *Nature*, 558, 586–589.

Boynton, W. V., Taylor, G. J., Evans, L. G., Reedy, R. C., Starr, R., Janes, D. M., Kerry, K. E., Drake, D. M., Kim, K. J., Williams, R. M. S., Crombie, M. K., Dohm, J. M., Baker, V., Metzger, A. E., Karunatillake, S., Keller, J. M., Newsom, H. E., Arnold, J. R., Brückner, J., Englert, P. A. J., Gasnault, O., Sprague, A. L., Mitrofanov, I., Squyres, S. W., Trombka, J. I., d'Uston, L., Wänke, H., and Hamara, D. K. (2007). Concentration of H, Si, Cl, K, Fe, and Th in the low- and mid-latitude regions of Mars. *J. Geophys. Res.*, 112, article no. E12S99.

Briggs, R. M., Utting, A. J., and Gibson, I. L. (1990). The origin of alkaline magmas in an intraplate setting near a subduction zone: the Ngatutura Basalts, North Island, New Zealand. *J. Volcanol. Geotherm. Res.*, 40, 55–70.

Brophy, J. G. (1991). Composition gaps, critical crystallinity, and fractional crystallization in orogenic (calc-alkaline) magmatic systems. *Contrib. Mineral. Petrol.*, 109, 173–182.

Carr, M. H. and Head, J. W. (2010). Geologic history of Mars. *Earth Planet. Sci. Lett.*, 294, 185–203.

Carter, J. and Poulet, F. (2013). Ancient plutonic processes on Mars inferred from the detection of possible anorthositic terrains. *Nat. Geosci.*, 6, 1008–1012.

Christensen, P. R., Bandfield, J. L., Hamilton, V. E., Ruff, S. W., Kieffer, H. H., Titus, T. N., Malin, M. C., Morris, R. V., Lane, M. D., Clark, R. L., Jakosky, B. M., Mellon, M. T., Pearl, J. C., Conrath, B. J., Smith, M. D., Clancy, R. T., Kuzmin, R. O., Roush, T., Mehall, G. L., Gorelick, N., Bender, K., Murray, K., Dason, S., Greene, E., Silverman, S., and Greenfield, M. (2001). Mars global surveyor thermal emission spectrometer experiment: investigation description and surface science results. *J. Geophys.*

Res., 106, 23823–23871.

Christensen, P. R., Jakosky, B. M., Kieffer, H. H., Malin, M. C., McSween Jr, H., Nealson, K., Mehall, G., Silverman, S., Ferry, S., Caplinger, M., and Ravine, M. (2004). The thermal emission imaging system (THEMIS) for the Mars 2001 odyssey mission. *Space Sci. Rev.*, 110, 85–130.

Christensen, P. R., McSween, H. Y., Bandfield, J. L., Ruff, S. W., Rogers, A. D., Hamilton, V. E., Gorelick, N., Wyatt, M. B., Jakosky, B. M., Kieffer, H. H., Malin, M. C., and Moersch, J. E. (2005). Evidence for magmatic evolution and diversity on Mars from infrared observations. *Nature*, 436, 504–509.

Citron, R. I., Manga, M., and Tan, E. (2018). A hybrid origin of the Martian crustal dichotomy: Degree-1 convection antipodal to a giant impact. *Earth Planet. Sci. Lett.*, 491, 58–66.

Clayton, R. N. and Mayeda, T. K. (1983). Oxygen isotopes in eucrites, shergottites, nakhlites, and chassignites. *Earth Planet. Sci. Lett.*, 62, 1–6.

Clayton, R. N. and Mayeda, T. K. (1996). Oxygen isotope studies of achondrites. *Geochim. Cosmochim. Acta*, 60, 1999–2017.

Collinet, M., Médard, E., Charlier, B., Vander Auwera, J., and Grove, T. L. (2015). Melting of the primitive martian mantle at 0.5–22 GPa and the origin of basalts and alkaline rocks on Mars. *Earth Planet. Sci. Lett.*, 427, 83–94.

Connerney, J. E. P., Acuña, M. H., Ness, N. F., Kletetschka, G., Mitchell, D. L., Lin, R. P., and Reme, H. (2005). Tectonic implications of Mars crustal magnetism. *Proc. Natl. Acad. Sci. USA*, 102, 14970–14975.

Cousin, A., Sautter, V., Payré, V., Forni, O., Mangold, N., Gasnault, O., Le Deit, L., Johnson, J., Maurice, S., Salvatore, M., Wiens, R. C., Gasda, P., and Rapin, W. (2017). Classification of igneous rocks analyzed by ChemCam at Gale crater, Mars. *Icarus*, 288, 265–283.

Dauphas, N. and Pourmand, A. (2011). Hf–W–Th evidence for rapid growth of Mars and its status as a planetary embryo. *Nature*, 473, 489–492.

Debaille, V., Brandon, A. D., O'Neill, C., Yin, Q.-Z., and Jacobsen, B. (2009). Early martian mantle overturn inferred from isotopic composition of nakhlite meteorites. *Nat. Geosci.*, 2, 548–552.

Deng, Z., Moynier, F., Villeneuve, J., Jensen, N. K., Liu, D., Cartigny, P., Mikouchi, T., Siebert, J., Agranier, A., Chaussidon, M., and Bizzarro, M. (2020). Early oxidation of the martian crust triggered by impacts. *Sci. Adv.*, 6, article no. eabc4941.

Ehlmann, B. L. and Edwards, C. S. (2014). Mineralogy of the Martian surface. *Annu. Rev. Earth Planet. Sci.*, 42, 291–315.

Elkins-Tanton, L. T. (2008). Linked magma ocean solidification and atmospheric growth for Earth and Mars. *Earth Planet. Sci. Lett.*, 271, 181–191.

Elkins-Tanton, L. T., Zaranek, S. E., Parmentier, E. M., and Hess, P. C. (2005). Early magnetic field and magmatic activity on Mars from magma ocean cumulate overturn. *Earth Planet. Sci. Lett.*, 236, 1–12.

Eugster, O., Busemann, H., Lorenzetti, S., and Terribilini, D. (2002). Ejection ages from krypton-81-krypton-83 dating and pre-atmospheric sizes of martian meteorites. *Meteorit. Planet. Sci.*, 37, 1345–1360.

Farley, K. A., Malespin, C., Mahaffy, P., Grotzinger, J. P., Vasconcelos, P. M., Milliken, R. E., Malin, M., Edgett, K. S., Pavlov, A. A., Hurowitz, J. A., Grant, J. A., Miller, H. B., Arvidson, R., Beegle, L., Calef, F., Conrad, P. G., Dietrich, W. E., Eigenbrode, J., Gellert, R., Gupta, S., Hamilton, V., Hassler, D. M., Lewis, K. W., McLennan, S. M., Ming, D., Navarro-Gonzalez, R., Schwenzer, S. P., Steele, A., Stolper, E. M., Sumner, D. Y., Vaniman, D., Vasavada, A., Williford, K., Wimmer-Schweingruber, R. F., Team, the M.S.L.S., Blake, D. F., Bristow, T., DesMarais, D., Edwards, L., Haberle, R., Hoehler, T., Hollingsworth, J., Kahre, M., Keely, L., McKay, C., Wilhelm, M. B., Bleacher, L., Brinckerhoff, W., Choi, D., Dworkin, J. P., Floyd, M., Freissinet, C., Garvin, J., Glavin, D., Harpold, D., Martin, D. K., McAdam, A., Raaen, E., Smith, M. D., Stern, J., Tan, F., Trainer, M., Meyer, M., Posner, A., Voytek, M., Anderson, R. C., Aubrey, A., Behar, A., Blaney, D., Brinza, D., Christensen, L., Crisp, J. A., DeFlores, L., Feldman, J., Feldman, S., Flesch, G., Hurowitz, J., Jun, I., Keymeulen, D., Maki, J., Mischna, M., Morookian, J. M., Parker, T., Pavri, B., Schoppers, M., Sengstacken, A., Simmonds, J. J., Spanovich, N., Juarez, M. d. l. T., Webster, C. R., Yen, A., Archer, P. D., Cucinotta, F., Jones, J. H., Morris, R. V., Niles, P., Rampe, E., Nolan, T., Fisk, M., Radziemski, L., Barraclough, B., Bender, S., Berman, D., Dobrea, E. N., Tokar, R., Williams, R. M. E., Yingst, A., Leshin, L., Cleghorn, T., Huntress, W., Manhes, G., Hudgins, J., Olson, T., Stewart, N., Sarrazin, P., Vicenzi, E., Wilson, S. A.,

Bullock, M., Ehresmann, B., Peterson, J., Rafkin, S., Zeitlin, C., Fedosov, F., Golovin, D., Karpushkina, N., Kozyrev, A., Litvak, M., Malakhov, A., Mitrofanov, I., Mokrousov, M., Nikiforov, S., Prokhorov, V., Sanin, A., Tretyakov, V., Varenikov, A., Vostrukhin, A., Kuzmin, R., Clark, B., Wolff, M., Botta, O., Drake, D., Bean, K., Lemmon, M., Anderson, R. B., Herkenhoff, K., Lee, E. M., Sucharski, R., Hernandez, M. A. d. P., Avalos, J. J. B., Ramos, M., Kim, M.-H., Plante, I., Muller, J.-P., Ewing, R., Boynton, W., Downs, R., Fitzgibbon, M., Harshman, K., Morrison, S., Kortmann, O., Palucis, M., Williams, A., Lugmair, G., Wilson, M. A., Rubin, D., Jakosky, B., Balic-Zunic, T., Frydenvang, J., Jensen, J. K., Kinch, K., Koefoed, A., Madsen, M. B., Stipp, S. L. S., Boyd, N., Campbell, J. L., Perrett, G., Pradler, I., VanBommel, S., Jacob, S., Owen, T., Rowland, S., Savijarvi, H., Boehm, E., Bottcher, S., Burmeister, S., Guo, J., Kohler, J., Garcia, C. M., Mueller-Mellin, R., Bridges, J. C., McConnochie, T., Benna, M., Franz, H., Bower, H., Brunner, A., Blau, H., Boucher, T., Carmosino, M., Atreya, S., Elliott, H., Halleaux, D., Renno, N., Wong, M., Pepin, R., Elliott, B., Spray, J., Thompson, L., Gordon, S., Newsom, H., Ollila, A., Williams, J., Bentz, J., Nealson, K., Popa, R., Kah, L. C., Moersch, J., Tate, C., Day, M., Kocurek, G., Hallet, B., Sletten, R., Francis, R., McCullough, E., Cloutis, E., ten Kate, I. L., Kuzmin, R., Fraeman, A., Scholes, D., Slavney, S., Stein, T., Ward, J., Berger, J., and Moores, J. E. (2014). In situ radiometric and exposure age dating of the Martian surface. *Science*, 343, article no. 1247166.

Filiberto, J. (2017). Geochemistry of Martian basalts with constraints on magma genesis. *Chem. Geol.*, 466, 1–14.

Filiberto, J., Gross, J., and McCubbin, F. M. (2016). Constraints on the water, chlorine, and fluorine content of the Martian mantle. *Meteorit. Planet. Sci.*, 51, 2023–2035.

Flahaut, J., Quantin, C., Clenet, H., Allemand, P., Mustard, J. F., and Thomas, P. (2012). Pristine Noachian crust and key geologic transitions in the lower walls of Valles Marineris: Insights into early igneous processes on Mars. *Icarus*, 221, 420–435.

Foley, C. N., Economou, T., Clayton, R. N., and Dietrich, W. (2003). Calibration of the Mars Pathfinder alpha proton X-ray spectrometer. *J. Geophys. Res.*, 108(E12), article no. 8095.

Gellert, R., Berger, J. A., Boyd, N., Brunet, C., Campbell, J. L., Curry, M., Elliott, B., Fulford, P., Grotzinger, J., Hipkin, V., Hurowitz, J. A., King, P. L., Leshin, L. A., Limonadi, D., Pavri, B., Marchand, G., Perrett, G. M., Scodary, A., Simmonds, J. J., Spray, J., Squyres, S. W., Thompson, L., VanBommel, S., Pradler, I., Yen, A. S., and MSL Science Team (2013). Initial MSL APXS Activities and Observations at Gale Crater, Mars. In *The 44th Lunar and Planetary Science Conference Abs. Proceeding, Contribution*, page 1432.

Ghiorso, M. S., Hirschmann, M. M., Reiners, P. W., and Kress, V. C. (2002). The pMELTS: A revision of MELTS for improved calculation of phase relations and major element partitioning related to partial melting of the mantle to 3 GPa. *Geochem. Geophys. Geosystems*, 3, 1–35.

Greeley, R., Foing, B. H., McSween, H. Y., Neukum, G., Pinet, P., van Kan, M., Werner, S. C., Williams, D. A., and Zegers, T. E. (2005). Fluid lava flows in Gusev crater, Mars. *J. Geophys. Res. E*, 110, article no. E05008.

Gross, J., Treiman, A. H., Filiberto, J., and Herd, C. D. K. (2011). Primitive olivine-phyric shergottite NWA 5789: Petrology, mineral chemistry and cooling history imply a magma similar to Yamato 980459. *Meteorit. Planet. Sci.*, 46(1), 116–133.

Haltigin, T., Lange, C., Mugnuolo, R., Smith, C., Haltigin, T., Lange, C., Mugnolo, R., Smith, C., Amundsen, H., Bousquet, P., Conley, C., Debus, A., Dias, J., Falkner, P., Gass, V., Harri, A.-M., Hauber, E., Ivanov, A., Ivanov, A., Kminek, G., Korablev, O., Koschny, D., Larranaga, J., Marty, B., McLennan, S., Meyer, M., Nilsen, E., Orleanski, P., Orosei, R., Rebuffat, D., Safa, F., Schmitz, N., Siljeström, S., Thomas, N., Vago, J., Vandaele, A.-C., Voirin, T., and Whetsel, C. (2018). iMARS Phase 2. *Astrobiology*, 18, S1–S131.

Hamilton, V. E., McSween, H. Y., and Hapke, B. (2005). Mineralogy of Martian atmospheric dust inferred from thermal infrared spectra of aerosols. *J. Geophys. Res.*, 110, article no. E12006.

Hanna, K. L. D., Thomas, I. R., Bowles, N. E., Greenhagen, B. T., Pieters, C. M., Mustard, J. F., Jackson, C. R. M., and Wyatt, M. B. (2012). Laboratory emissivity measurements of the plagioclase solid solution series under varying environmental conditions. *J. Geophys. Res.*, 117. https://doi.org/10.1029/2012JE004184.

Harder, H. and Christensen, U. R. (1996). A one-plume model of martian mantle convection. *Na-*

ture, 380, 507–509.

Hartmann, W. K. and Neukum, G. (2001). Cratering chronology and the evolution of Mars. *Space Sci. Rev.*, 96, 165–194.

Hewins, R. H., Zanda, B., Humayun, M., Nemchin, A., Lorand, J.-P., Pont, S., Deldicque, D., Bellucci, J. J., Beck, P., Leroux, H., Marinova, M., Remusat, L., Göpel, C., Lewin, E., Grange, M., Kennedy, A., and Whitehouse, M. J. (2017). Regolith breccia Northwest Africa 7533: Mineralogy and petrology with implications for early Mars. *Meteorit. Planet. Sci.*, 52, 89–124.

Humayun, M., Nemchin, A., Zanda, B., Hewins, R. H., Grange, M., Kennedy, A., Lorand, J.-P., Göpel, C., Fieni, C., Pont, S., and Deldicque, D. (2013). Origin and age of the earliest Martian crust from meteorite NWA 7533. *Nature*, 503, 513–516.

Kamber, B. S., Whitehouse, M. J., Bolhar, R., and Moorbath, S. (2005). Volcanic resurfacing and the early terrestrial crust: Zircon U-Pb and REE constraints from the Isua Greenstone Belt, southern West Greenland. *Earth Planet. Sci. Lett.*, 240, 276–290.

Karunatillake, S., Wray, J. J., Gasnault, O., McLennan, S. M., Rogers, A. D., Squyres, S. W., Boynton, W. V., Skok, J. R., Ojha, L., and Olsen, N. (2014). Sulfates hydrating bulk soil in the Martian low and middle latitudes. *Geophys. Res. Lett.*, 41, 7987–7996.

Karunatillake, S., Wray, J. J., Squyres, S. W., Taylor, G. J., Gasnault, O., McLennan, S. M., Boyton, W., El Maarry, M. R., and Dohm, J. M. (2009). Chemically striking regions on Mars and Stealth revisited. *J. Geophys. Res.*, 114, article no. E12001.

Kiefer, W. S. (2003). Melting in the martian mantle: Shergottite formation and implications for present-day mantle convection on Mars. *Meteorit. Planet. Sci.*, 38, 1815–1832.

Koeppen, W. C. and Hamilton, V. E. (2008). Global distribution, composition, and abundance of olivine on the surface of Mars from thermal infrared data. *J. Geophys. Res.*, 113, article no. E05001.

Lapen, T. J., Righter, M., Andreasen, R., Irving, A. J., Satkoski, A. M., Beard, B. L., Nishiizumi, K., Jull, A. J. T., and Caffee, M. W. (2017). Two billion years of magmatism recorded from a single Mars meteorite ejection site. *Sci. Adv.*, 3, article no. e1600922.

Lapen, T. J., Righter, M., Brandon, A. D., Debaille, V., Beard, B. L., Shafer, J. T., and Peslier, A. H. (2010). A younger age for ALH84001 and its geochemical link to Shergottite sources in Mars. *Science*, 328, 347–351.

Le Deit, L., Hauber, E., Fueten, F., Pondrelli, M., Rossi, A. P., and Jaumann, R. (2013). Sequence of infilling events in gale crater, Mars: Results from morphology, stratigraphy, and mineralogy. *J. Geophys. Res. E*, 118, 2439–2473.

Lognonné, P., Banerdt, W. B., Giardini, D., Pike, W. T., Christensen, U., Laudet, P., de Raucourt, S., Zweifel, P., Calcutt, S., Bierwirth, M., Hurst, K. J., Ijpelaan, F., Umland, J. W., Llorca-Cejudo, R., Larson, S. A., Garcia, R. F., Kedar, S., Knapmeyer-Endrun, B., Mimoun, D., Mocquet, A., Panning, M. P., Weber, R. C., Sylvestre-Baron, A., Pont, G., Verdier, N., Kerjean, L., Facto, L. J., Gharakanian, V., Feldman, J. E., Hoffman, T. L., Klein, D. B., Klein, K., Onufer, N. P., Paredes-Garcia, J., Petkov, M. P., Willis, J. R., Smrekar, S. E., Drilleau, M., Gabsi, T., Nebut, T., Robert, O., Tillier, S., Moreau, C., Parise, M., Aveni, G., Ben Charef, S., Bennour, Y., Camus, T., Dandonneau, P. A., Desfoux, C., Lecomte, B., Pot, O., Revuz, P., Mance, D., tenPierick, J., Bowles, N. E., Charalambous, C., Delahunty, A. K., Hurley, J., Irshad, R., Liu, H., Mukherjee, A. G., Standley, I. M., Stott, A. E., Temple, J., Warren, T., Eberhardt, M., Kramer, A., Kühne, W., Miettinen, E.-P., Monecke, M., Aicardi, C., André, M., Baroukh, J., Borrien, A., Bouisset, A., Boutte, P., Brethomé, K., Brysbaert, C., Carlier, T., Deleuze, M., DesMarres, J. M., Dilhan, D., Doucet, C., Faye, D., Faye-Refalo, N., Gonzalez, R., Imbert, C., Larigauderie, C., Locatelli, E., Luno, L., Meyer, J.-R., Mialhe, F., Mouret, J. M., Nonon, M., Pahn, Y., Paillet, A., Pasquier, P., Perez, G., Perez, R., Perrin, L., Pouilloux, B., Rosak, A., Savin de Larclause, I., Sicre, J., Sodki, M., Toulemont, N., Vella, B., Yana, C., Alibay, F., Avalos, O. M., Balzer, M. A., Bhandari, P., Blanco, E., Bone, B. D., Bousman, J. C., Bruneau, P., Calef, F. J., Calvet, R. J., D'Agostino, S. A., de los Santos, G., Deen, R. G., Denise, R. W., Ervin, J., Ferraro, N. W., Gengl, H. E., Grinblat, F., Hernandez, D., Hetzel, M., Johnson, M. E., Khachikyan, L., Lin, J. Y., Madzunkov, S. M., Marshall, S. L., Mikellides, I. G., Miller, E. A., Raff, W., Singer, J. E., Sunday, C. M., Villalvazo, J. F., Wallace, M. C., Banfield, D., Rodriguez-Manfredi, J. A., Russell, C. T., Trebi-Ollennu, A., Maki, J. N., Beucler, E., Böse, M., Bonjour, C., Berenguer, J. L., Ceylan, S., Clinton, J., Conejero, V., Daubar, I., Dehant, V., Delage, P., Euchner, F., Estève, I., Fayon, L., Ferraioli, L., Johnson,

C. L., Gagnepain-Beyneix, J., Golombek, M., Khan, A., Kawamura, T., Kenda, B., Labrot, P., Murdoch, N., Pardo, C., Perrin, C., Pou, L., Sauron, A., Savoie, D., Stähler, S., Stutzmann, E., Teanby, N. A., Tromp, J., van Driel, M., Wieczorek, M., Widmer-Schnidrig, R., and Wookey, J. (2019). SEIS: insight's seismic experiment for internal structure of Mars. *Space Sci. Rev.*, 215, article no. 12.

Mangold, N., Schmidt, M. E., Fisk, M. R., Forni, O., McLennan, S. M., Ming, D. W., Sautter, V., Sumner, D., Williams, A. J., Clegg, S. M., Cousin, A., Gasnault, O., Gellert, R., Grotzinger, J. P., and Wiens, R. C. (2017). Classification scheme for sedimentary and igneous rocks in Gale crater, Mars. *Icarus*, 284, 1–17.

Marchi, S., Bottke, W. F., Elkins-Tanton, L. T., Bierhaus, M., Wuennemann, K., Morbidelli, A., and Kring, D. A. (2014). Widespread mixing and burial of Earth's Hadean crust by asteroid impacts. *Nature*, 511, 578–582.

Maurice, S., Wiens, R. C., Saccoccio, M., Barraclough, B., Gasnault, O., Forni, O., Mangold, N., Baratoux, D., Bender, S., Berger, G., Bernardin, J., Berthé, M., Bridges, N., Blaney, D., Bouyé, M., Caïs, P., Clark, B., Clegg, S., Cousin, A., Cremers, D., Cros, A., DeFlores, L., Derycke, C., Dingler, B., Dromart, G., Dubois, B., Dupieux, M., Durand, E., d'Uston, L., Fabre, C., Faure, B., Gaboriaud, A., Gharsa, T., Herkenhoff, K., Kan, E., Kirkland, L., Kouach, D., Lacour, J.-L., Langevin, Y., Lasue, J., Le Mouélic, S., Lescure, M., Lewin, E., Limonadi, D., Manhès, G., Mauchien, P., McKay, C., Meslin, P.-Y., Michel, Y., Miller, E., Newsom, H. E., Orttner, G., Paillet, A., Parès, L., Parot, Y., Pérez, R., Pinet, P., Poitrasson, F., Quertier, B., Sallé, B., Sotin, C., Sautter, V., Séran, H., Simmonds, J. J., Sirven, J.-B., Stiglich, R., Striebig, N., Thocaven, J.-J., Toplis, M. J., and Vaniman, D. (2012). The ChemCam instrument suite on the Mars science laboratory (MSL) rover: Science objectives and mast unit description. *Space Sci. Rev.*, 170, 95–166.

McCoy, T. J., Sims, M., Schmidt, M. E., Edwards, L., Tornabene, L. L., Crumpler, L. S., Cohen, B. A., Soderblom, L. A., Blaney, D. L., Squyres, S. W., Arvidson, R. E., Rice, J. W., Tréguier, E., d'Uston, C., Grant, J. A., McSween, H. Y., Golombek, M. P., Haldemann, A. F. C., and de Souza, P. A. (2008). Structure, stratigraphy, and origin of Husband Hill, Columbia Hills, Gusev Crater, Mars. *J. Geophys. Res.*, 113, article no. E06S03.

McCubbin, F. M., Boyce, J. W., Novak-Szabo, T., Santos, A., Tartese, R., Muttik, N., Domokos, G., Vazquez, J. A., Keller, L. P., Moser, D. E., Jerolmack, D. J., Shearer, C. K., Steele, A., Elardo, S. M., Rahman, Z., Anand, M., Delhaye, T., and Agee, C. B. (2016a). Geologic history of Martian regolith breccia Northwest Africa 7034: Evidence for hydrothermal activity and lithologic diversity in the Martian crust. *J. Geophys. Res. E*, 121, 2120–2149.

McCubbin, F. M., Boyce, J. W., Srinivasan, P., Santos, A. R., Elardo, S. M., Filiberto, J., Steele, A., and Shearer, C. K. (2016b). Heterogeneous distribution of H2O in the Martian interior: Implications for the abundance of H2O in depleted and enriched mantle sources. *Meteorit. Planet. Sci.*, 51, 2036–2060.

McCubbin, F. M., Hauri, E. H., Elardo, S. M., Kaaden, K. E. V., Wang, J., and Shearer, C. K. (2012). Hydrous melting of the martian mantle produced both depleted and enriched shergottites. *Geology*, 40, 683–686.

McSween, H. Y. (2015). Petrology on Mars. *Am. Mineral.*, 100, 2380–2395.

McSween, H. Y., Grove, T. L., and Wyatt, M. B. (2003). Constraints on the composition and petrogenesis of the Martian crust. *J. Geophys. Res.*, 108(E12), article no. 5135.

McSween, H. Y., Murchie, S. L., Crisp, J. A., Bridges, N. T., Anderson, R. C., Bell, J. F., Britt, D. T., Brückner, J., Dreibus, G., Economou, T., Ghosh, A., Golombek, M. P., Greenwood, J. P., Johnson, J. R., Moore, H. J., Morris, R. V., Parker, T. J., Rieder, R., Singer, R., and Wänke, H. (1999). Chemical, multispectral, and textural constraints on the composition and origin of rocks at the Mars Pathfinder landing site. *J. Geophys. Res.*, 104, 8679–8715.

McSween, H. Y., Ruff, S. W., Morris, R. V., Bell, J. F., Herkenhoff, K., Gellert, R., Stockstill, K. R., Tornabene, L. L., Squyres, S. W., Crisp, J. A., Christensen, P. R., McCoy, T. J., Mittlefehldt, D. W., and Schmidt, M. (2006a). Alkaline volcanic rocks from the Columbia Hills, Gusev crater, Mars. *J. Geophys. Res.*, 111, article no. E09S91.

McSween, H. Y., Taylor, G. J., and Wyatt, M. B. (2009). Elemental composition of the Martian crust. *Science*, 324, 736–739.

McSween, H. Y., Wyatt, M. B., Gellert, R., Bell, J. F., Morris, R. V., Herkenhoff, K. E., Crumpler, L. S., Milam, K. A., Stockstill, K. R., Tornabene, L. L.,

Arvidson, R. E., Bartlett, P., Blaney, D., Cabrol, N. A., Christensen, P. R., Clark, B. C., Crisp, J. A., Des Marais, D. J., Economou, T., Farmer, J. D., Farrand, W., Ghosh, A., Golombek, M., Gorevan, S., Greeley, R., Hamilton, V. E., Johnson, J. R., Joliff, B. L., Klingelhöfer, G., Knudson, A. T., McLennan, S., Ming, D., Moersch, J. E., Rieder, R., Ruff, S. W., Schröder, C., de Souza, P. A., Squyres, S. W., Wänke, H., Wang, A., Yen, A., and Zipfel, J. (2006b). Characterization and petrologic interpretation of olivine-rich basalts at Gusev Crater, Mars. *J. Geophys. Res.*, 111, article no. E02S10.

Meslin, P.-Y., Gasnault, O., Forni, O., Schroder, S., Cousin, A., Berger, G., Clegg, S. M., Lasue, J., Maurice, S., Sautter, V., Le Mouelic, S., Wiens, R. C., Fabre, C., Goetz, W., Bish, D., Mangold, N., Ehlmann, B., Lanza, N., Harri, A.-M., Anderson, R., Rampe, E., McConnochie, T. H., Pinet, P., Blaney, D., Leveille, R., Archer, D., Barraclough, B., Bender, S., Blake, D., Blank, J. G., Bridges, N., Clark, B. C., DeFlores, L., DeLapp, D., Dromart, G., Dyar, M. D., Fisk, M., Gondet, B., Grotzinger, J., Herkenhoff, K., Johnson, J., Lacour, J.-L., Langevin, Y., Leshin, L., Lewin, E., Madsen, M. B., Melikechi, N., Mezzacappa, A., Mischna, M. A., Moores, J. E., Newsom, H., Ollila, A., Perez, R., Renno, N., Sirven, J.-B., Tokar, R., de la Torre, M., d'Uston, L., Vaniman, D., Yingst, A., MSL Science Team, Kemppinen, O., Minitti, M., Cremers, D., Bell, J. F., Edgar, L., Farmer, J., Godber, A., Wadhwa, M., Wellington, D., McEwan, I., Newman, C., Richardson, M., Charpentier, A., Peret, L., King, P., Weigle, G., Schmidt, M., Li, S., Milliken, R., Robertson, K., Sun, V., Baker, M., Edwards, C., Farley, K., Griffes, J., Miller, H., Newcombe, M., Pilorget, C., Rice, M., Siebach, K., Stack, K., Stolper, E., Brunet, C., Hipkin, V., Marchand, G., Sanchez, P. S., Favot, L., Cody, G., Steele, A., Fluckiger, L., Lees, D., Nefian, A., Martin, M., Gailhanou, M., Westall, F., Israel, G., Agard, C., Baroukh, J., Donny, C., Gaboriaud, A., Guillemot, P., Lafaille, V., Lorigny, E., Paillet, A., Perez, R., Saccoccio, M., Yana, C., Armiens-Aparicio, C., Rodriguez, J. C., Blazquez, I. C., Gomez, F. G., Gomez-Elvira, J., Hettrich, S., Malvitte, A. L., Jimenez, M. M., Martinez-Frias, J., Martin-Soler, J., Martin-Torres, F. J., Jurado, A. M., Mora-Sotomayor, L., Caro, G. M., Lopez, S. N., Peinado-Gonzalez, V., Pla-Garcia, J., Manfredi, J. A. R., Romeral-Planello, J. J., Fuentes, S. A. S., Martinez, E. S., Redondo, J. T., Urqui-O'Callaghan, R., Mier, M.-P. Z., Chipera, S., Mauchien, P., Manning, H., Fairen, A., Hayes, A., Joseph, J., Squyres, S., Sullivan, R., Thomas, P., Dupont, A., Lundberg, A., DeMarines, J., Grinspoon, D., Reitz, G., Prats, B., Atlaskin, E., Genzer, M., Haukka, H., Kahanpaa, H., Kauhanen, J., Kemppinen, O., Paton, M., Polkko, J., Schmidt, W., Siili, T., Wray, J., Wilhelm, M. B., Poitrasson, F., Patel, K., Gorevan, S., Indyk, S., Paulsen, G., Gupta, S., Schieber, J., Geffroy, C., Baratoux, D., Cros, A., Lee, Q.-M., Pallier, E., Parot, Y., Toplis, M., Brunner, W., Heydari, E., Achilles, C., Oehler, D., Sutter, B., Cabane, M., Coscia, D., Israel, G., Szopa, C., Robert, F., Nachon, M., Buch, A., Stalport, F., Coll, P., Francois, P., Raulin, F., Teinturier, S., Cameron, J., Dingler, R., Jackson, R. S., Johnstone, S., Little, C., Nelson, T., Williams, R. B., Jones, A., Kirkland, L., Treiman, A., Baker, B., Cantor, B., Caplinger, M., Davis, S., Duston, B., Edgett, K., Fay, D., Hardgrove, C., Harker, D., Herrera, P., Jensen, E., Kennedy, M. R., Krezoski, G., Krysak, D., Lipkaman, L., Malin, M., McCartney, E., McNair, S., Nixon, B., Posiolova, L., Ravine, M., Salamon, A., Saper, L., Stoiber, K., Supulver, K., Van Beek, J., Van Beek, T., Zimdar, R., French, K. L., Iagnemma, K., Miller, K., Summons, R., Goesmann, F., Hviid, S., Johnson, M., Lefavor, M., Lyness, E., Breves, E., Fassett, C., Bristow, T., DesMarais, D., Edwards, L., Haberle, R., Hoehler, T., Hollingsworth, J., Kahre, M., Keely, L., McKay, C., Wilhelm, M. B., Bleacher, L., Brinckerhoff, W., Choi, D., Conrad, P., Dworkin, J. P., Eigenbrode, J., Floyd, M., Freissinet, C., Garvin, J., Glavin, D., Harpold, D., Jones, A., Mahaffy, P., Martin, D. K., McAdam, A., Pavlov, A., Raaen, E., Smith, M. D., Stern, J., Tan, F., Trainer, M., Meyer, M., Posner, A., Voytek, M., Anderson, R. C., Aubrey, A., Beegle, L. W., Behar, A., Brinza, D., Calef, F., Christensen, L., Crisp, J. A., Feldman, J., Feldman, S., Flesch, G., Hurowitz, J., Jun, I., Keymeulen, D., Maki, J., Morookian, J. M., Parker, T., Pavri, B., Schoppers, M., Sengstacken, A., Simmonds, J. J., Spanovich, N., Vasavada, A. R., Webster, C. R., Yen, A., Cucinotta, F., Jones, J. H., Ming, D., Morris, R. V., Niles, P., Nolan, T., Radziemski, L., Berman, D., Dobrea, E. N., Williams, R. M. E., Lewis, K., Cleghorn, T., Huntress, W., Manhes, G., Hudgins, J., Olson, T., Stewart, N., Sarrazin, P., Grant, J., Vicenzi, E., Wilson, S. A., Bullock, M., Ehresmann, B., Hamilton, V., Hassler, D., Peterson, J., Rafkin,

S., Zeitlin, C., Fedosov, F., Golovin, D., Karpushkina, N., Kozyrev, A., Litvak, M., Malakhov, A., Mitrofanov, I., Mokrousov, M., Nikiforov, S., Prokhorov, V., Sanin, A., Tretyakov, V., Varenikov, A., Vostrukhin, A., Kuzmin, R., Wolff, M., McLennan, S., Botta, O., Drake, D., Bean, K., Lemmon, M., Schwenzer, S. P., Lee, E. M., Sucharski, R., Hernandez, M. A. d. P., Avalos, J. J. B., Ramos, M., Kim, M.-H., Malespin, C., Plante, I., Muller, J.-P., Navarro-Gonzalez, R., Ewing, R., Boynton, W., Downs, R., Fitzgibbon, M., Harshman, K., Morrison, S., Dietrich, W., Kortmann, O., Palucis, M., Sumner, D. Y., Williams, A., Lugmair, G., Wilson, M. A., Rubin, D., Jakosky, B., Balic-Zunic, T., Frydenvang, J., Jensen, J. K., Kinch, K., Koefoed, A., Stipp, S. L. S., Boyd, N., Campbell, J. L., Gellert, R., Perrett, G., Pradler, I., VanBommel, S., Jacob, S., Owen, T., Rowland, S., Atlaskin, E., Savijarvi, H., Boehm, E., Bottcher, S., Burmeister, S., Guo, J., Kohler, J., Garcia, C. M., Mueller-Mellin, R., Wimmer-Schweingruber, R., Bridges, J. C., Benna, M., Franz, H., Bower, H., Brunner, A., Blau, H., Boucher, T., Carmosino, M., Atreya, S., Elliott, H., Halleaux, D., Renno, N., Wong, M., Pepin, R., Elliott, B., Spray, J., Thompson, L., Gordon, S., Williams, J., Vasconcelos, P., Bentz, J., Nealson, K., Popa, R., Kah, L. C., Moersch, J., Tate, C., Day, M., Kocurek, G., Hallet, B., Sletten, R., Francis, R., McCullough, E., Cloutis, E., ten Kate, I. L., Kuzmin, R., Arvidson, R., Fraeman, A., Scholes, D., Slavney, S., Stein, T., Ward, J., and Berger, J. (2013). Soil diversity and hydration as observed by ChemCam at Gale crater, Mars. *Science*, 341, article no. 1238670.

Ming, D. W., Gellert, R., Morris, R. V., Arvidson, R. E., Brückner, J., Clark, B. C., Cohen, B. A., d'Uston, C., Economou, T., Fleischer, I., Klingelhöfer, G., McCoy, T. J., Mittlefehldt, D. W., Schmidt, M. E., Schröder, C., Squyres, S. W., Tréguier, E., Yen, A. S., and Zipfel, J. (2008). Geochemical properties of rocks and soils in Gusev crater, Mars: Results of the alpha particle X-ray spectrometer from Cumberland Ridge to home plate. *J. Geophys. Res.*, 113(E12), article no. E12S39.

Ming, D. W., Mittlefehldt, D. W., Morris, R. V., Golden, D. C., Gellert, R., Yen, A., Clark, B. C., Squyres, S. W., Farrand, W. H., Ruff, S. W., Arvidson, R. E., Klingelhofer, G., McSween, H. Y., Rodionov, D. S., Schroder, C., de Souza Jr., P. A., and Wang, A. (2006). Geochemical and mineralogical indicators of aqueous processes in the Columbia Hills of Gusev crater, Mars. *J. Geophys. Res.*, 111, article no. E072S12.

Mittlefehldt, D. W. (1994). ALH84001, a cumulate orthopyroxenite member of the martian meteorite clan. *Meteoritics*, 29, 214–221.

Murchie, S., Arvidson, R., Bedini, P., Beisser, K., Bibring, J.-P., Bishop, J., Boldt, J., Cavender, P., Choo, T., Clancy, R. T., Darlington, E. H., Des Marais, D., Espiritu, R., Fort, D., Green, R., Guinness, E., Hayes, J., Hash, C., Heffernan, K., Hemmler, J., Heyler, G., Humm, D., Hutcheson, J., Izenberg, N., Lee, R., Lees, J., Lohr, D., Malaret, E., Martin, T., McGovern, J. A., McGuire, P., Morris, R., Mustard, J., Pelkey, S., Rhodes, E., Robinson, M., Roush, T., Schaefer, E., Seagrave, G., Seelos, F., Silverglate, P., Slavney, S., Smith, M., Shyong, W.-J., Strohbehn, K., Taylor, H., Thompson, P., Tossman, B., Wirzburger, M., and Wolff, M. (2007). Compact reconnaissance imaging spectrometer for Mars (CRISM) on Mars reconnaissance orbiter (MRO). *J. Geophys. Res.*, 112, article no. E05S03.

Mustard, J. F., Poulet, F., Gendrin, A., Bibring, J.-P., Langevin, Y., Gondet, B., Mangold, N., Bellucci, G., and Altieri, F. (2005). Olivine and pyroxene diversity in the crust of Mars. *Science*, 307, 1594–1597.

Nekvasil, H., Filiberto, J., McCubbin, F. M., and Lindsley, D. H. (2007). Alkalic parental magmas for chassignites? *Meteorit. Planet. Sci.*, 42, 979–992.

Nekvasil, H., Simon, A., and Lindsley, D. H. (2000). Crystal fractionation and the evolution of intraplate hy-normative igneous suites: Insights from their Feldspars. *J. Petrol.*, 41, 1743–1757.

Nemchin, A., Timms, N., Pidgeon, R., Geisler, T., Reddy, S., and Meyer, C. (2009). Timing of crystallization of the lunar magma ocean constrained by the oldest zircon. *Nat. Geosci.*, 2, 133–136.

Nyquist, L. E., Bogard, D. D., Shih, C.-Y., Greshake, A., Stöffler, D., and Eugster, O. (2001). Ages and Geologic Histories of Martian Meteorites. In *Chronology and Evolution of Mars, Space Sciences Series of ISSI*, pages 105–164. Springer, Dordrecht.

Nyquist, L. E., Shih, C.-Y., McCubbin, F. M., Santos, A. R., Shearer, C. K., Peng, Z. X., Burger, P. V., and Agee, C. B. (2016). Rb–Sr and Sm–Nd isotopic and REE studies of igneous components in the bulk matrix domain of Martian breccia Northwest Africa 7034. *Meteorit. Planet. Sci.*, 51, 483–498.

Ody, A., Poulet, F., Bibring, J.-P., Loizeau, D., Carter, J., Gondet, B., and Langevin, Y. (2013). Global investigation of olivine on Mars: Insights into crust and

mantle composition. *J. Geophys. Res.: Planets*, 118, 234–262.

Ostwald, A. M., Udry, A., Gazel, E., and Payre, V. (2020). Assimilation-fractional crystallization on Mars as a formation process for Felsic rocks. In *51st Lunar and Planetary Science Conference*.

Palme, H. and O'Neill, H. S. C. (2014). Cosmochemical estimates of mantle composition. In Holland, H. D. and Turekian, K. K., editors, *Treatise on Geochemistry*, pages 1–39. Elsevier, Oxford, 2nd edition.

Payré, V., Fabre, C., Cousin, A., Sautter, V., Wiens, R. C., Forni, O., Gasnault, O., Mangold, N., Meslin, P.-Y., Lasue, J., Ollila, A., Rapin, W., Maurice, S., Nachon, M., Le Deit, L., Lanza, N., and Clegg, S. (2017). Alkali trace elements in Gale crater, Mars, with ChemCam: Calibration update and geological implications. *J. Geophys. Res.*, 122, 650–679.

Payré, V., Siebach, K. L., Dasgupta, R., Udry, A., Rampe, E. B., and Morrison, S. M. (2020). Constraining ancient magmatic evolution on Mars using crystal chemistry of detrital igneous minerals in the sedimentary Bradbury Group, Gale crater, Mars. *J. Geophys. Res.*, 125, article no. e2020JE006467.

Poulet, F., Mangold, N., Platevoet, B., Bardintzeff, J.-M., Sautter, V., Mustard, J. F., Bibring, J.-P., Pinet, P., Langevin, Y., Gondet, B., and Aléon-Toppani, A. (2009). Quantitative compositional analysis of martian mafic regions using the MEx/OMEGA reflectance data: 2 Petrological implications. *Icarus*, 201, 84–101.

Rice, M. S., Gupta, S., Treiman, A. H., Stack, K. M., Calef, F., Edgar, L. A., Grotzinger, J., Lanza, N., Le Deit, L., Lasue, J., Siebach, K. L., Vasavada, A., Wiens, R. C., and Williams, J. (2017). Geologic overview of the Mars science laboratory Rover mission at the Kimberley, Gale crater, Mars: Overview of MSL at the Kimberley. *J. Geophys. Res.*, 122, 2–20.

Riu, L., Poulet, F., Bibring, J.-P., and Gondet, B. (2019). The M3 project: 2 — Global distributions of mafic mineral abundances on Mars. *Icarus*, 322, 31–53.

Rogers, A. D. and Nazarian, A. H. (2013). Evidence for Noachian flood volcanism in Noachis Terra, Mars, and the possible role of Hellas impact basin tectonics. *J. Geophys. Res.: Planets*, 118(5), 1094–1113.

Rogers, A. D. and Nekvasil, H. (2015). Feldspathic rocks on Mars: Compositional constraints from infrared spectroscopy and possible formation mechanisms: Feldspathic rocks on Mars: constraints. *Geophys. Res. Lett.*, 42, 2619–2626.

Ruff, S. W., Christensen, P. R., Blaney, D. L., Farrand, W. H., Johnson, J. R., Michalski, J. R., Moersch, J. E., Wright, S. P., and Squyres, S. W. (2006). The rocks of Gusev crater as viewed by the Mini-TES instrument. *J. Geophys. Res.*, 111. https://doi.org/10.1029/2006JE002747.

Santos, A. R., Agee, C. B., McCubbin, F. M., Shearer, C. K., Burger, P. V., Tartèse, R., and Anand, M. (2015). Petrology of igneous clasts in Northwest Africa 7034: Implications for the petrologic diversity of the martian crust. *Geochim. Cosmochim. Acta*, 157, 56–85.

Sautter, V., Fabre, C., Forni, O., Toplis, M. J., Cousin, A., Ollila, A. M., Meslin, P. Y., Maurice, S., Wiens, R. C., Baratoux, D., Mangold, N., Le Mouélic, S., Gasnault, O., Berger, G., Lasue, J., Anderson, R. A., Lewin, E., Schmidt, M., Dyar, D., Ehlmann, B. L., Bridges, J., Clark, B., and Pinet, P. (2014). Igneous mineralogy at Bradbury rise: The first ChemCam campaign at Gale crater. *J. Geophys. Res.*, 119, 30–46.

Sautter, V., Toplis, M. J., Beck, P., Mangold, N., Wiens, R., Pinet, P., Cousin, A., Maurice, S., LeDeit, L., Hewins, R., Gasnault, O., Quantin, C., Forni, O., Newsom, H., Meslin, P.-Y., Wray, J., Bridges, N., Payré, V., Rapin, W., and Le Mouélic, S. (2016). Magmatic complexity on early Mars as seen through a combination of orbital, in-situ and meteorite data. *Lithos*, 254–255, 36–52.

Sautter, V., Toplis, M. J., Wiens, R. C., Cousin, A., Fabre, C., Gasnault, O., Maurice, S., Forni, O., Lasue, J., Ollila, A., Bridges, J. C., Mangold, N., Le Mouélic, S., Fisk, M., Meslin, P.-Y., Beck, P., Pinet, P., Le Deit, L., Rapin, W., Stolper, E. M., Newsom, H., Dyar, D., Lanza, N., Vaniman, D., Clegg, S., and Wray, J. J. (2015). In situ evidence for continental crust on early Mars. *Nat. Geosci.*, 8, 605–609.

Schmidt, M. E., Campbell, J. L., Gellert, R., Perret, G. M., Treimann, A. H., Blaney, D. L., Ollila, A., Calef, F. J., Edgar, L., Elliot, B. E., Grotzinger, J., Hurowitz, J., King, P. L., Minetti, M. E., Sautter, V., Stack, K., Berger, J. A., Bridges, J. C., Ehlman, B. L., Forni, O., Leshin, L. A., Lewis, K. W., McLennan, S. M., Ming, D. W., Newson, H., Squyres, S. W., Stolper, E. M., Thopson, L., VanBommel, S., Wiens, R., and MSL Science Team (2014). Geochemical diversity in the first rocks examined by Curiosity

rover in Gale Crater: evidence for and significance of an alkali and volatile-rich igneous source. *J. Geophys. Res.: Planets*, 119, 64–81.

Schmidt, M. E., Izawa, M. R. M., Thomas, A. P., Thompson, L., and Gellert, R. (2016). Diverse Igneous Protolith Contributions to Sediments in Gale Crater: Variable Metasomatism of the Mars Mantle. *Meteorit. Planet. Sci.*, 51(A555), article no. 6074.

Schmidt, M. E. and McCoy, T. J. (2010). The evolution of a heterogeneous Martian mantle: Clues from K, P, Ti, Cr, and Ni variations in Gusev basalts and shergottite meteorites. *Earth Planet. Sci. Lett.*, 296, 67–77.

Squyres, S. W., Aharonson, O., Clark, B. C., Cohen, B. A., Crumpler, L., de Souza, P. A., Farrand, W. H., Gellert, R., Grant, J., Grotzinger, J. P., Haldemann, A. F. C., Johnson, J. R., Klingelhofer, G., Lewis, K. W., Li, R., McCoy, T., McEwen, A. S., McSween, H. Y., Ming, D. W., Moore, J. M., Morris, R. V., Parker, T. J., Rice, J. W., Ruff, S., Schmidt, M., Schroder, C., Soderblom, L., and Yen, A. (2007). Pyroclastic activity at home plate in Gusev crater, Mars. *Science*, 316, 738–742.

Squyres, S. W., Arvidson, R. E., Blaney, D. L., Clark, B. C., Crumpler, L., Farrand, W. H., Gorevan, S., Herkenhoff, K. E., Hurowitz, J., Kusack, A., McSween, H. Y., Ming, D. W., Morris, R. V., Ruff, S. W., Wang, A., and Yen, A. (2006). Rocks of the Columbia Hills: Rocks of the Columbia Hills. *J. Geophys. Res.*, 111, article no. EO2S11.

Stolper, E. M., Baker, M. B., Newcombe, M. E., Schmidt, M. E., Treiman, A. H., Cousin, A., Dyar, M. D., Fisk, M. R., Gellert, R., King, P. L., Leshin, L., Maurice, S., McLennan, S. M., Minitti, M. E., Perrett, G., Rowland, S., Sautter, V., Wiens, R. C., MSL Science Team, Kemppinen, O., Bridges, N., Johnson, J. R., Cremers, D., Bell, J. F., Edgar, L., Farmer, J., Godber, A., Wadhwa, M., Wellington, D., McEwan, I., Newman, C., Richardson, M., Charpentier, A., Peret, L., Blank, J., Weigle, G., Li, S., Milliken, R., Robertson, K., Sun, V., Edwards, C., Ehlmann, B., Farley, K., Griffes, J., Grotzinger, J., Miller, H., Pilorget, C., Rice, M., Siebach, K., Stack, K., Brunet, C., Hipkin, V., Leveille, R., Marchand, G., Sanchez, P. S., Favot, L., Cody, G., Steele, A., Fluckiger, L., Lees, D., Nefian, A., Martin, M., Gailhanou, M., Westall, F., Israel, G., Agard, C., Baroukh, J., Donny, C., Gaboriaud, A., Guillemot, P., Lafaille, V., Lorigny, E., Paillet, A., Perez, R., Saccoccio, M., Yana, C., Armiens-Aparicio, C., Rodriguez, J. C., Blazquez, I. C., Gomez, F. G., Gomez-Elvira, J., Hettrich, S., Malvitte, A. L., Jimenez, M. M., Martinez-Frias, J., Martin-Soler, J., Martin-Torres, F. J., Jurado, A. M., Mora-Sotomayor, L., Caro, G. M., Lopez, S. N., Peinado-Gonzalez, V., Pla-Garcia, J., Manfredi, J. A. R., Romeral-Planello, J. J., Fuentes, S. A. S., Martinez, E. S., Redondo, J. T., Urqui-O'Callaghan, R., Mier, M.-P. Z., Chipera, S., Lacour, J.-L., Mauchien, P., Sirven, J.-B., Manning, H., Fairen, A., Hayes, A., Joseph, J., Squyres, S., Sullivan, R., Thomas, P., Dupont, A., Lundberg, A., Melikechi, N., Mezzacappa, A., DeMarines, J., Grinspoon, D., Reitz, G., Prats, B., Atlaskin, E., Genzer, M., Harri, A.-M., Haukka, H., Kahanpaa, H., Kauhanen, J., Kemppinen, O., Paton, M., Polkko, J., Schmidt, W., Siili, T., Fabre, C., Wray, J., Wilhelm, M. B., Poitrasson, F., Patel, K., Gorevan, S., Indyk, S., Paulsen, G., Gupta, S., Bish, D., Schieber, J., Gondet, B., Langevin, Y., Geffroy, C., Baratoux, D., Berger, G., Cros, A., d'Uston, C., Forni, O., Gasnault, O., Lasue, J., Lee, Q.-M., Meslin, P.-Y., Pallier, E., Parot, Y., Pinet, P., Schroder, S., Toplis, M., Lewin, E., Brunner, W., Heydari, E., Achilles, C., Oehler, D., Sutter, B., Cabane, M., Coscia, D., Israel, G., Szopa, C., Teinturier, S., Dromart, G., Robert, F., Le Mouelic, S., Mangold, N., Nachon, M., Buch, A., Stalport, F., Coll, P., Francois, P., Raulin, F., Cameron, J., Clegg, S., DeLapp, D., Dingler, R., Jackson, R. S., Johnstone, S., Lanza, N., Little, C., Nelson, T., Williams, R. B., Kirkland, L., Baker, B., Cantor, B., Caplinger, M., Davis, S., Duston, B., Edgett, K., Fay, D., Hardgrove, C., Harker, D., Herrera, P., Jensen, E., Kennedy, M. R., Krezoski, G., Krysak, D., Lipkaman, L., Malin, M., McCartney, E., McNair, S., Nixon, B., Posiolova, L., Ravine, M., Salamon, A., Saper, L., Stoiber, K., Supulver, K., Van Beek, J., Van Beek, T., Zimdar, R., French, K. L., Iagnemma, K., Miller, K., Summons, R., Goesmann, F., Goetz, W., Hviid, S., Johnson, M., Lefavor, M., Lyness, E., Breves, E., Fassett, C., Blake, D. F., Bristow, T., DesMarais, D., Edwards, L., Haberle, R., Hoehler, T., Hollingsworth, J., Kahre, M., Keely, L., McKay, C., Wilhelm, M. B., Bleacher, L., Brinckerhoff, W., Choi, D., Conrad, P., Dworkin, J. P., Eigenbrode, J., Floyd, M., Freissinet, C., Garvin, J., Glavin, D., Harpold, D., Mahaffy, P., Martin, D. K., McAdam, A., Pavlov, A., Raaen, E., Smith, M. D., Stern, J., Tan, F., Trainer, M., Meyer, M., Posner, A., Voytek, M., Anderson, R. C., Aubrey, A., Beegle, L. W., Behar, A., Blaney,

D., Brinza, D., Calef, F., Christensen, L., Crisp, J., DeFlores, L., Ehlmann, B., Feldman, J., Feldman, S., Flesch, G., Hurowitz, J., Jun, I., Keymeulen, D., Maki, J., Mischna, M., Morookian, J. M., Parker, T., Pavri, B., Schoppers, M., Sengstacken, A., Simmonds, J. J., Spanovich, N., Juarez, M. d. l. T., Vasavada, A., Webster, C. R., Yen, A., Archer, P. D., Cucinotta, F., Jones, J. H., Ming, D., Morris, R. V., Niles, P., Rampe, E., Nolan, T., Radziemski, L., Barraclough, B., Bender, S., Berman, D., Dobrea, E. N., Tokar, R., Vaniman, D., Williams, R. M. E., Yingst, A., Lewis, K., Cleghorn, T., Huntress, W., Manhes, G., Hudgins, J., Olson, T., Stewart, N., Sarrazin, P., Grant, J., Vicenzi, E., Wilson, S. A., Bullock, M., Ehresmann, B., Hamilton, V., Hassler, D., Peterson, J., Rafkin, S., Zeitlin, C., Fedosov, F., Golovin, D., Karpushkina, N., Kozyrev, A., Litvak, M., Malakhov, A., Mitrofanov, I., Mokrousov, M., Nikiforov, S., Prokhorov, V., Sanin, A., Tretyakov, V., Varenikov, A., Vostrukhin, A., Kuzmin, R., Clark, B., Wolff, M., Botta, O., Drake, D., Bean, K., Lemmon, M., Schwenzer, S. P., Anderson, R. B., Herkenhoff, K., Lee, E. M., Sucharski, R., Hernandez, M. A. d. P., Avalos, J. J. B., Ramos, M., Jones, A., Kim, M.-H., Malespin, C., Plante, I., Muller, J.-P., Navarro-Gonzalez, R., Ewing, R., Boynton, W., Downs, R., Fitzgibbon, M., Harshman, K., Morrison, S., Dietrich, W., Kortmann, O., Palucis, M., Sumner, D. Y., Williams, A., Lugmair, G., Wilson, M. A., Rubin, D., Jakosky, B., Balic-Zunic, T., Frydenvang, J., Jensen, J. K., Kinch, K., Koefoed, A., Madsen, M. B., Stipp, S. L. S., Boyd, N., Campbell, J. L., Pradler, I., VanBommel, S., Jacob, S., Owen, T., Atlaskin, E., Savijarvi, H., Boehm, E., Bottcher, S., Burmeister, S., Guo, J., Kohler, J., Garcia, C. M., Mueller-Mellin, R., Wimmer-Schweingruber, R., Bridges, J. C., McConnochie, T., Benna, M., Franz, H., Bower, H., Brunner, A., Blau, H., Boucher, T., Carmosino, M., Atreya, S., Elliott, H., Halleaux, D., Renno, N., Wong, M., Pepin, R., Elliott, B., Spray, J., Thompson, L., Gordon, S., Newsom, H., Ollila, A., Williams, J., Vasconcelos, P., Bentz, J., Nealson, K., Popa, R., Kah, L. C., Moersch, J., Tate, C., Day, M., Kocurek, G., Hallet, B., Sletten, R., Francis, R., McCullough, E., Cloutis, E., ten Kate, I. L., Kuzmin, R., Arvidson, R., Fraeman, A., Scholes, D., Slavney, S., Stein, T., Ward, J., Berger, J., and Moores, J. E. (2013). The Petrochemistry of Jake_M: A Martian Mugearite. *Science*, 341, article no. 1239463.

Tanaka, K. L., Robbins, S. J., Fortezzo, C. M., Skinner, J. A., and Hare, T. M. (2014). The digital global geologic map of Mars: Chronostratigraphic ages, topographic and crater morphologic characteristics, and updated resurfacing history. *Planet. Space Sci.*, 95, 11–24.

Tartèse, R., Anand, M., McCubbin, F. M., Santos, A. R., and Delhaye, T. (2014). Zircons in Northwest Africa 7034: Recorders of crustal evolution on Mars. In *The 45th Lunar and Planetary Science Conference Abs Procceding, Contribution*, page 2020.

Taylor, G. J., Martel, L. M. V., Karunatillake, S., Gasnault, O., and Boyton, W. V. (2010). Mapping Mars geochemically. *Geology*, 38, 183–186.

Taylor, S. R. and McLennan, S. (2009). *Planetary Crusts: Their Composition, Origin and Evolution*. Cambridge University Press, Cambridge.

Thiriet, M., Michaut, C., Breuer, D., and Plesa, A.-C. (2018). Hemispheric dichotomy in Lithosphere thickness on Mars caused by differences in crustal structure and composition. *J. Geophys. Res.*, 123, 823–848.

Thomas-Keprta, K. L., Clemett, S. J., McKay, D. S., Gibson, E. K., and Wentworth, S. J. (2009). Origins of magnetite nanocrystals in Martian meteorite ALH 84001. *Geochim. Cosmochim. Acta*, 73, 6631–6677.

Treiman, A. H. and Medard, E. (2016). Mantle metasomatism in Mars: Potassic basaltic sandstone in gale crater derived from partial melt of phlogopite-peridotite. In *GSA Annual Meeting in Denver, Colorado, USA, 2016*. article no. 285851.

Udry, A., Balta, J. B., and McSween, H. Y. (2014). Exploring fractionation models for Martian magmas: Fractionation of Martian primary magmas. *J. Geophys. Res.*, 119, 1–18.

Udry, A., Gazel, E., and McSween, H. Y. (2018). Formation of evolved rocks at Gale crater by crystal fractionation and implications for Mars crustal composition. *J. Geophys. Res.*, 123, 1525–1540.

Udry, A., Howarth, G. H., Herd, C. D. K., Day, J. M. D., Lapen, T. J., and Filiberto, J. (2020). What martian meteorites reveal about the interior and surface of Mars. *J. Geophys. Res.*, 125, article no. e2020JE006523.

Valley, J. W., Cavosie, A. J., Ushikubo, T., Reinhard, D. A., Lawrence, D. F., Larson, D. J., Clifton, P. H., Kelly, T. F., Wilde, S. A., Moser, D. E., and Spicuzza, M. J. (2014). Hadean age for a post-magma-ocean

zircon confirmed by atom-probe tomography. *Nat. Geosci.*, 7, 219–223.

Valley, J. W., King, E. M., Peck, W. H., Graham, C. M., and Wilde, S. A. (2001). The Cool Early Earth: Oxygen Isotope Evidence for Continental Crust and Oceans on Earth at 4.4 Ga. In *AGU Spring Meet. Abstr. V51A-01*.

Wanke, H. and Dreibus, G. (1988). Chemical composition and accretion history of terrestrial planets. *Philos. Trans. Royal Soc. A*, 325, 545–557.

Wieczorek, M. A. and Zuber, M. T. (2004). Thickness of the Martian crust: Improved constraints from geoid-to-topography ratios. *J. Geophys. Res.*, 109, article no. E01009.

Wiens, R. C., Maurice, S., Barraclough, B., Saccoccio, M., Barkley, W. C., Bell, J. F., Bender, S., Bernardin, J., Blaney, D., Blank, J., Bouyé, M., Bridges, N., Bultman, N., Caïs, P., Clanton, R. C., Clark, B., Clegg, S., Cousin, A., Cremers, D., Cros, A., DeFlores, L., DeLapp, D., Dingler, R., D'Uston, C., Darby Dyar, M., Elliott, T., Enemark, D., Fabre, C., Flores, M., Forni, O., Gasnault, O., Hale, T., Hays, C., Herkenhoff, K., Kan, E., Kirkland, L., Kouach, D., Landis, D., Langevin, Y., Lanza, N., LaRocca, F., Lasue, J., Latino, J., Limonadi, D., Lindensmith, C., Little, C., Mangold, N., Manhes, G., Mauchien, P., McKay, C., Miller, E., Mooney, J., Morris, R. V., Morrison, L., Nelson, T., Newsom, H., Ollila, A., Ott, M., Pares, L., Perez, R., Poitrasson, F., Provost, C., Reiter, J. W., Roberts, T., Romero, F., Sautter, V., Salazar, S., Simmonds, J. J., Stiglich, R., Storms, S., Striebig, N., Thocaven, J.-J., Trujillo, T., Ulibarri, M., Vaniman, D., Warner, N., Waterbury, R., Whitaker, R., Witt, J., and Wong-Swanson, B. (2012). The ChemCam instrument suite on the Mars science laboratory (MSL) Rover: Body unit and combined system tests. *Space Sci. Rev.*, 170, 167–227.

Wilde, S. A., Valley, J. W., Peck, W. H., and Graham, C. M. (2001). Evidence from detrital zircons for the existence of continental crust and oceans on the Earth 4.4 Gyr ago. *Nature*, 409, 175–178.

Winter, L. S., Tosdal, R. M., Mortensen, J. K., and Franklin, J. M. (2010). Volcanic stratigraphy and geochronology of the cretaceous lancones basin, Northwestern Peru: Position and timing of giant VMS deposits. *Econ. Geol.*, 105, 713–742.

Wittmann, A., Korotev, R. L., Jolliff, B. L., Irving, A. J., Moser, D. E., Barker, I., and Rumble, D. (2015). Petrography and composition of Martian regolith breccia meteorite Northwest Africa 7475. *Meteorit. Planet. Sci.*, 50, 326–352.

Wray, J. J., Hansen, S. T., Dufek, J., Swayze, G. A., Murchie, S. L., Seelos, F. P., Skok, J. R., Irwin, R. P., and Ghiorso, M. S. (2013). Prolonged magmatic activity on Mars inferred from the detection of felsic rocks. *Nat. Geosci.*, 6, 1013–1017.

Wray, J. J., Milliken, R. E., Dundas, C. M., Swayze, G. A., Andrews-Hanna, J. C., Baldridge, A. M., Chojnacki, M., Bishop, J. L., Ehlmann, B. L., Murchie, S. L., Clark, R. N., Seelos, F. P., Tornabene, L. L., and Squyres, S. W. (2011). Columbus crater and other possible groundwater-fed paleolakes of Terra Sirenum, Mars. *J. Geophys. Res.*, 116, article no. E01001.

Wyatt, M. B., McSween, H. Y., Tanaka, K. L., and Head, J. W. (2004). Global geologic context for rock types and surface alteration on Mars. *Geology*, 32, 645–648.

Xiao, L., Huang, J., Christensen, P. R., Greeley, R., Williams, D. A., Zhao, J., and He, Q. (2012). Ancient volcanism and its implication for thermal evolution of Mars. *Earth Planet. Sci. Lett.*, 323-324, 9–18.